# RESEARCH MEMORANDUM

## EFFECTS OF TWO LEADING-EDGE MODIFICATIONS ON THE AERODYNAMIC CHARACTERISTICS OF A THIN LOW-ASPECT-RATIO DELTA WING AT TRANSONIC SPEEDS

By John P. Mugler, Jr.

Langley Aeronautical Laboratory
Langley Field, Va.



NATIONAL ADVISORY COMMITTEE
FOR AERONAUTICS

WASHINGTON
October 12, 1956

NATIONAL ADVISORY COMMITTEE FOR AERONAUTICS

RESEARCH MEMORANDUM

# EFFECTS OF TWO LEADING-EDGE MODIFICATIONS ON THE AERODYNAMIC CHARACTERISTICS OF A THIN LOW-ASPECT-RATIO DELTA WING AT TRANSONIC SPEEDS

By John P. Mugler, Jr.

## SUMMARY

An investigation was conducted in the Langley 8-foot transonic tunnel to determine the aerodynamic characteristics of a thin 60° delta wing with two leading-edge modifications (conical leading-edge camber and leading-edge droop) in combination with bodies with and without body indentation in accordance with the transonic-area-rule concept. The tests covered a Mach number range from 0.60 to 1.15 and an angle-of-attack range from -4° to 20° at a Reynolds number of about $3 \times 10^6$ based on the wing mean aerodynamic chord. The wing had an aspect ratio of 2.31, a taper ratio of 0, and, without modifications, had NACA 65A003 airfoil sections parallel to the model plane of symmetry.

Conical camber designed for a lift coefficient of 0.15 near $M \approx 1.0$ over the leading-edge portion of the wing is more effective than $2\frac{1}{2}^\circ$ of leading-edge droop in reducing the drag at lift. Increases in maximum lift-drag ratio of the order of 22 percent are obtained at subsonic speeds with conical camber, diminishing to about a 10-percent increase at transonic speeds. Body indentation is effective in delaying the transonic drag rise to a higher Mach number.

## INTRODUCTION

It has been realized that, theoretically, the low-aspect ratio flat wing of triangular plan form with full leading-edge suction approaches minimum induced drag (ref. 1). Experimentally, however, the rather sharp leading edges on thin wings produce very high induced velocities which cause leading-edge flow separation resulting in increased drag. Previous wind-tunnel investigations (refs. 2 and 3) have shown that reducing the angle of attack of the leading-edge portion of the wing can be effective

[redacted]

in reducing the flow separation and in addition cause a beneficial thrust or suction force to be realized over the leading-edge portion of the wing. This paper presents the results of an investigation to ascertain the effectiveness of leading-edge droop and conical camber on a thin 60° delta wing in obtaining more beneficial suction in the transonic Mach number range. Since aerodynamic gains are being obtained through the application of the transonic area rule, a study of the effects of body indentation on one of the modified wing models is included.

## SYMBOLS

| | |
|---|---|
| $A$ | aspect ratio |
| $M$ | free-stream Mach number |
| $C_L$ | lift coefficient, $\frac{\text{Lift}}{qS}$ |
| $C_D$ | drag coefficient, $\frac{\text{Drag}}{qS}$ |
| $C_m$ | pitching-moment coefficient, $\frac{\text{Pitching moment about } \bar{c}/4}{qS\bar{c}}$ |
| $(L/D)_{max}$ | maximum value of lift-drag ratio |
| $C_{L,(L/D)_{max}}$ | lift coefficient at $(L/D)_{max}$ |
| $S$ | total wing area of wing with pointed tips |
| $\bar{c}$ | wing mean aerodynamic chord, $\frac{2}{S}\int_0^{b/2} c^2 dy$ |
| $q$ | free-stream dynamic pressure |
| $\alpha$ | angle of attack of body center line |

[redacted]

## APPARATUS AND METHODS

### Tunnel

The subject investigation was conducted in the Langley 8-foot transonic tunnel, which is a dodecagonal slotted-throat, single-return wind tunnel operated at atmospheric stagnation pressures. The flow in the region of the test section occupied by the model was satisfactorily uniform at all test Mach numbers (ref. 4).

### Models

The plane delta wing tested has 60° sweepback of the leading edge, a taper ratio of 0, and NACA 65A003 airfoil sections parallel to the model plane of symmetry. The actual wing deviated from the theoretical delta plan form in that the wing tips were rounded. Rounding the tips reduced the wing area by a small amount (a reduction of 0.6 percent of total wing area) and produced negligible changes in mean aerodynamic chord length and location. The theoretical aspect ratio, which assumes pointed wing tips, is 2.31. The wing was constructed of steel and was tested as a midwing configuration. Dimensional details of the plane wing-body combination are presented in figure 1(a).

The drooped-leading-edge wing was obtained by modifying the leading-edge portion of the plane wing as shown in figure 1(b). Effectively, this modification drooped the forward 1.2 inches of the wing about $2\frac{1}{2}^{\circ}$ in the streamwise direction over the entire span. Upon completion of the tests on the wing with the drooped leading edge, the wing leading edge was again modified to incorporate conical camber over the outboard 15 percent of each semispan. The amount of the leading-edge line vertical displacement at any spanwise station (denoted Z, fig. 1(c)) was obtained from reference 5 for a lift coefficient of 0.15 near $M = 1.0$. The data of reference 5 were computed using the method of reference 2. Then a parabolic mean camber line was fitted in the streamwise direction between the displaced leading edge and a line at 85 percent of the local semispan. Next, the thickness distribution of the plane wing was sheared vertically until it was distributed evenly about the parabolic mean line. Details of this modification are shown in figure 1(c).

The wing with plane, drooped, and conical cambered leading edges was tested in combination with a body of revolution designed to have minimum wave drag for a given length and volume (Sears-Haack body). The rear portion of the bodies was cut off to accommodate a three component internal strain-gage balance. However, the body tested with the plane and drooped

leading edges, designated the original body, was cut off at body station 31.7; whereas, the body tested with the conical cambered leading-edge wing, designated the basic body, was cut off at body station 35.3 (fig. 1(a)). The location of the wing with respect to the body nose was unchanged. The effects of lengthening the body in this manner on the significant aerodynamic parameters will be discussed in a later section.

The indented bodies for design Mach numbers of 1.0 and 1.2 tested in combination with the cambered leading-edge wing were obtained in accordance with the area-rule concepts (refs. 6 and 7). However, the indentations were made to a body slightly larger than the basic body, designated the modified body, instead of the basic body. This modification to the basic body consisted of increasing the maximum body diameter from 3.212 inches to 3.296 inches. Increasing the maximum diameter in this way added a small amount of volume to the body in the region of the wing (table II, ref. 8). The effects of this modification will also be discussed in a later section. Table I presents the coordinates for all bodies tested. Figure 2 presents photographs of two of the configurations tested.

The model was attached to an internal strain-gage balance. The downstream end of the balance was attached to an axial support tube through a sting. Couplings between the sting and axial support tube were varied to keep the model near the center of the tunnel at all angles of attack.

## Measurements and Accuracy

A study of the factors affecting the accuracy of the results indicates that the measured coefficients are accurate within the following limits:

| M | $C_L$ | $C_D$ | $C_m$ |
|---|---|---|---|
| 0.60 | 0.025 | 0.0015 | 0.005 |
| 1.15 | .012 | .0010 | .003 |

The average free-stream Mach number was determined to within $\pm 0.003$ from a calibration with respect to the pressure in the chamber surrounding the slotted test section.

The angle of attack of the model was measured with a strain-gage attitude transmitter mounted in the model nose. A consideration of factors affecting the accuracy of this measurement indicates that the model angle of attack is accurate to within $\pm 0.1^\circ$.

[redacted]

## Configurations and Test Conditions

Seven configurations tested during this investigation and the test conditions are given in the following table:

| Configuration | Description | Angle-of-attack range, deg | Mach number range | Remarks |
|---|---|---|---|---|
| 1 | Plane delta wing in combination with original body | 0 to 12 (a) | 0.80 to 1.15 | |
| 2 | Drooped leading-edge delta wing in combination with basic body | 0 to 12 (a) | 0.80 to 1.15 | |
| 3 | Conical cambered leading-edge delta wing in combination with basic body | -4 to 20 | 0.60 to 1.12 | |
| 4 | Conical cambered leading-edge delta wing in combination with basic body | -4 to 20 | 0.60 to 1.12 | Transition fixed |
| 5 | Conical cambered leading-edge delta wing in combination with M = 1.0 indented body | -4 to 20 | 0.60 to 1.12 | |
| 6 | Conical cambered leading-edge delta wing in combination with M = 1.2 indented body | -4 to 20 | 0.60 to 1.12 | |
| 7 | Conical cambered leading-edge delta wing in combination with M = 1.2 indented body | -4 to 20 | 0.60 to 1.12 | Transition fixed |

[a]Except at M = 1.15.

The Reynolds number based on the wing mean aerodynamic chord was of the order of $3 \times 10^6$.

On configurations 4 and 7 where transition was fixed, the transition consisted of No. 120 size carborundum strips approximately 0.10 inch wide placed at 10 percent of the wing chord (upper and lower surface) and around the model nose at 10 percent of the body length.

## Corrections

No corrections have been applied to the data for boundary-interference effects. At subsonic speeds, the slotted test section minimized boundary-interference effects such as blockage and boundary-induced upwash. At Mach numbers between 1.03 and 1.12, boundary-reflected disturbances struck the model so no data were recorded in this Mach number range.

The drag data have been adjusted to the condition of free-stream static pressure at the base of the body.

## RESULTS

Force and moment characteristics for the plane and drooped leading-edge wing in combination with the original body are presented in figures 3 and 4, respectively. Figures 5 to 7 present similar data for the conical cambered leading-edge wing in combination with the basic body with and without transition, the $M = 1.0$ indented body, and the $M = 1.2$ indented body with and without transition, respectively. The data used to show the effects of leading-edge modifications, body indentation, and transition on the aerodynamic parameters, figures 8, 9, and 10, respectively, were obtained from the faired curves of force and moment coefficients.

In figures 3 and 4, too few data points were recorded at moderate lift to define the curves. In figures 5 to 7, considerably more data points were recorded in this range; however, in many instances the regions of discontinuity still lacked precise definition. Therefore, the fairings in the region are approximate. Abrupt changes of this nature in the force and moment curves at moderate lift are characteristic of delta-wing—body configurations (i.e., ref. 9).

The theoretical values of maximum lift-drag ratio presented in figure 8(b) were obtained from the relation $1/2\sqrt{1/KC_{D_0}}$, where $C_{D_0}$ is the drag coefficient at zero lift for the plane wing. For full leading-edge suction, the drag-due-to-lift factor $K$ for subsonic speeds was taken as $1/\pi A$ and for supersonic speeds was obtained from reference 10. For no leading-edge suction, $K$ was taken as $\dfrac{1}{57.3\left(\dfrac{\partial C_L}{\partial \alpha}\right)_{C_L=0}}$ for the entire Mach number range.

In order to facilitate presentation of the data, staggered scales have been used in many figures and care should be taken in selecting the zero axis for each curve.

## DISCUSSION

### Effects of Leading-Edge Modifications

No corrections have been applied to the data of figure 8 to account for the longer body tested with the cambered-leading-edge wing or to the data of figure 9 to account for the modification to the basic body before the indentations were made. Body-alone tests of the original, basic, and modified bodies, reported in reference 8, show the effect on drag coefficient at zero angle of attack of these body modifications. These data indicate that the effects are small and will not significantly affect any of the trends or the validity of the comparisons made in figures 8 and 9.

The effects of the leading-edge modifications on the drag are presented in figure 8(a). As might be expected, the drag at zero lift of the plane wing is less than that for either the drooped or cambered leading-edge wings. At lift coefficients of 0.2 and 0.4, both modifications are responsible for reductions in drag. Leading-edge droop is effective in reducing the drag at lift at subsonic speeds, but this benefit diminishes rapidly with increases in Mach number. Conical leading-edge camber, however, is responsible for about an 18-percent reduction in drag at subsonic speeds at a lift coefficient of 0.2, and maintains a reduction of the order of 8 percent through the transonic speed range. At a lift coefficient of 0.4, the magnitude of the drag reduction due to conical camber is about 8 percent and is approximately constant throughout the Mach number range.

Since the leading-edge droop is effective in reducing the drag at lift only at subsonic speeds, the resulting increases in maximum lift-drag ratios due to leading-edge droop are limited to that Mach number range (fig. 8(b)). Conical leading-edge camber, on the other hand, is effective in increasing the maximum lift-drag ratios to some degree over the entire Mach number range tested. At a Mach number of 0.8 a maximum increase in maximum lift-drag ratio of 22 percent is realized but this increase diminishes to about a 10-percent increase at transonic speeds. The leading-edge modifications have little effect on the lift coefficient at which the maximum lift-drag ratios occur (fig. 8(b)).

In order to evaluate the effectiveness of the leading-edge modifications tested, the theoretical full and no leading-edge suction values were put on figure 8(b). At a Mach number of 0.80, the conical cambered leading-edge wing obtains about 42 percent of full leading-edge suction. This is a considerable improvement over the plane or drooped leading-edge wing; however, other unpublished data indicate that it is possible to obtain a considerably greater percentage of full leading-edge suction by detailed changes in the camber design.

The effects of the leading-edge modifications on the lift-curve slope and static longitudinal stability parameter are generally small. (See fig. 8(c).) Leading-edge droop causes a slight decrease in lift-curve slope in the transonic Mach number range and both leading-edge modifications are responsible for a small increase in static longitudinal stability below a Mach number of about 1.0. At supersonic speeds, however, leading-edge droop was responsible for a sizable decrease in static longitudinal stability.

## Effects of Body Indentation

Figure 9 presents the effects of body indentation on the aerodynamic characteristics of the cambered leading-edge configuration. The significant effect of body indentation is to delay the transonic drag rise to a higher Mach number (fig. 9(a)). This delay results in drag reductions of the order of 10 percent around $M = 1.0$. Generally, the body indented for $M = 1.0$ was slightly more effective in causing this delay than the body indented for $M = 1.2$. Since the addition of the thin wing to the body did not appreciably increase the drag rise over the drag rise of the body alone, the drag rise at zero lift was reduced only slightly by body indentation. The result of the delay in the transonic drag rise on the maximum lift-drag ratio characteristics (fig. 9(b)) is to cause a corresponding delay in the Mach number where the maximum lift-drag ratio decreases to the supersonic value. Body indentation has very little effect on the lift coefficient at which the maximum lift-drag ratios occur.

## Effect of Transition

The effects of fixing transition on the cambered leading-edge configurations are shown in figure 10. Generally, fixing transition increased the drag level slightly through the range of variables tested. Calculations based on the test Reynolds number of $3 \times 10^6$, assuming the skin friction of the model equal to the skin friction of a flat plate of the same wetted area, indicate that the flow was fully turbulent without transition. These calculated and experimental results are consistent since the addition of transition to an already turbulent flow is likely to cause a slight increase in drag.

## SUMMARY OF RESULTS

An investigation of the effects of two leading-edge modifications on the aerodynamic characteristics of a thin $60^\circ$ delta wing in combination with basic and indented bodies has been conducted in the 8-foot

transonic tunnel. The data have been analyzed and indicate the following results:

1. Conical leading-edge camber designed for a lift coefficient of 0.15 near $M = 1.0$ is more effective in reducing the drag at lift and increasing the maximum lift-drag ratio than $2\frac{1}{2}^\circ$ of leading-edge droop. Considerable benefits from conical camber are realized throughout the Mach number range. The benefits from leading-edge droop are smaller and are realized only at subsonic speeds.

2. Body indentation is effective in delaying the transonic drag rise to a higher Mach number, which affords a drag reduction around a Mach number of 1.0.

Langley Aeronautical Laboratory,
National Advisory Committee for Aeronautics,
Langley Field, Va., June 29, 1956.

REFERENCES

1. Jones, Robert T.: Properties of Low-Aspect-Ratio Pointed Wings at Speeds Below and Above the Speed of Sound. NACA Rep. 835, 1946. (Supersedes NACA TN 1032.)

2. Hall, Charles F., and Heitmeyer, John Charles: Lift, Drag, and Pitching Moment of Low-Aspect-Ratio Wings at Subsonic and Supersonic Speeds - Twisted and Cambered Triangular Wing of Aspect Ratio 2 With NACA 0003-63 Thickness Distribution. NACA RM A51E01, 1951.

3. Burrows, Dale L., and Palmer, William E.: A Transonic Wind-Tunnel Investigation of the Force and Moment Characteristics of a Plane and a Cambered 3-Percent-Thick Delta Wing of Aspect Ratio 3 on a Slender Body. NACA RM L54H25, 1954.

4. Ritchie, Virgil S., and Pearson, Albin O.: Calibration of the Slotted Test Section of the Langley 8-Foot Transonic Tunnel and Preliminary Experimental Investigation of Boundary-Reflected Disturbances. NACA RM L51K14, 1952.

5. Burnett, H. R.: Geometry of Cambered Leading Edges and Warped Tips To Be Evaluated in the NACA 8 Ft. and 4 × 4 Ft. Tunnels for the F-102 Airplane. Aero. Memo. A-8-44 (Contract no. AF33(600)-5942), Consolidated Vultee Aircraft Corp., May 27, 1953.

6. Whitcomb, Richard T.: A Study of the Zero-Lift Drag-Rise Characteristics of Wing-Body Combinations Near the Speed of Sound. NACA RM L52H08, 1952.

7. Whitcomb, Richard T., and Fischetti, Thomas L.: Development of a Supersonic Area Rule and an Application to the Design of a Wing-Body Combination Having High Lift-To-Drag Ratios. NACA RM L53H31a, 1953.

8. Loving, Donald L.: A Transonic Investigation of Changing Indentation Design Mach Number on the Aerodynamic Characteristics of a 45° Sweptback-Wing—Body Combination Designed for High Performance. NACA RM L55J07, 1956.

9. Mugler, John P., Jr.: Transonic Wind-Tunnel Investigation of the Aerodynamic Loading Characteristics of a 60° Delta Wing in the Presence of a Body With and Without Indentation. NACA RM L55G11, 1955.

10. Brown, Clinton E.: Theoretical Lift and Drag of Thin Triangular Wings at Supersonic Speeds. NACA Rep. 839, 1946. (Supersedes NACA TN 1183.)

[redacted]

TABLE I

BODY COORDINATES

| Station, in. from nose | Radius, in., for - | | | |
|---|---|---|---|---|
| | Original body (used in combination with plane and drooped-leading-edge wing) | Basic body (used in combination with cambered-leading-edge wing) | Indented bodies (used in combination with the cambered-leading-edge wing) | |
| | | | M = 1.0 | M = 1.2 |
| 0 | 0 | 0 | 0 | 0 |
| 1 | .282 | .282 | .282 | .282 |
| 2 | .460 | .460 | .460 | .460 |
| 3 | .612 | .612 | .612 | .612 |
| 4 | .743 | .743 | .743 | .743 |
| 5 | .862 | .862 | .862 | .862 |
| 6 | .969 | .969 | .969 | .969 |
| 7 | 1.062 | 1.062 | 1.062 | 1.062 |
| 8 | 1.150 | 1.150 | 1.150 | 1.150 |
| 9 | 1.222 | 1.222 | 1.222 | 1.222 |
| 10 | 1.290 | 1.290 | 1.290 | 1.290 |
| 11 | 1.350 | 1.350 | 1.350 | 1.350 |
| 12 | 1.404 | 1.404 | 1.404 | 1.404 |
| 13 | 1.452 | 1.452 | 1.454 | 1.454 |
| 14 | 1.493 | 1.493 | 1.499 | 1.499 |
| 15 | 1.526 | 1.526 | 1.540 | 1.535 |
| 16 | 1.552 | 1.552 | 1.560 | 1.551 |
| 17 | 1.575 | 1.575 | 1.560 | 1.553 |
| 18 | 1.590 | 1.590 | 1.553 | 1.541 |
| 19 | 1.602 | 1.602 | 1.536 | 1.523 |
| 20 | 1.606 | 1.606 | 1.505 | 1.502 |
| 21 | 1.602 | 1.602 | 1.464 | 1.466 |
| 22 | 1.594 | 1.594 | 1.425 | 1.444 |
| 23 | 1.578 | 1.578 | 1.391 | 1.433 |
| 24 | 1.560 | 1.560 | 1.378 | 1.431 |
| 25 | 1.532 | 1.532 | 1.381 | 1.431 |
| 26 | 1.501 | 1.501 | 1.413 | 1.423 |
| 27 | 1.460 | 1.460 | 1.443 | 1.405 |
| 28 | 1.414 | 1.414 | 1.414 | 1.381 |
| 29 | 1.360 | 1.360 | 1.360 | 1.339 |
| 30 | 1.300 | 1.300 | 1.300 | 1.287 |
| 31 | 1.231 | 1.231 | 1.231 | 1.227 |
| 31.7 | 1.182 | 1.182 | 1.182 | 1.182 |
| 32 | | 1.158 | 1.158 | 1.158 |
| 33 | | 1.076 | 1.076 | 1.076 |
| 34 | | 0.984 | 0.984 | 0.984 |
| 35 | | 0.878 | 0.878 | 0.878 |
| 35.3 | | 0.844 | 0.844 | 0.844 |

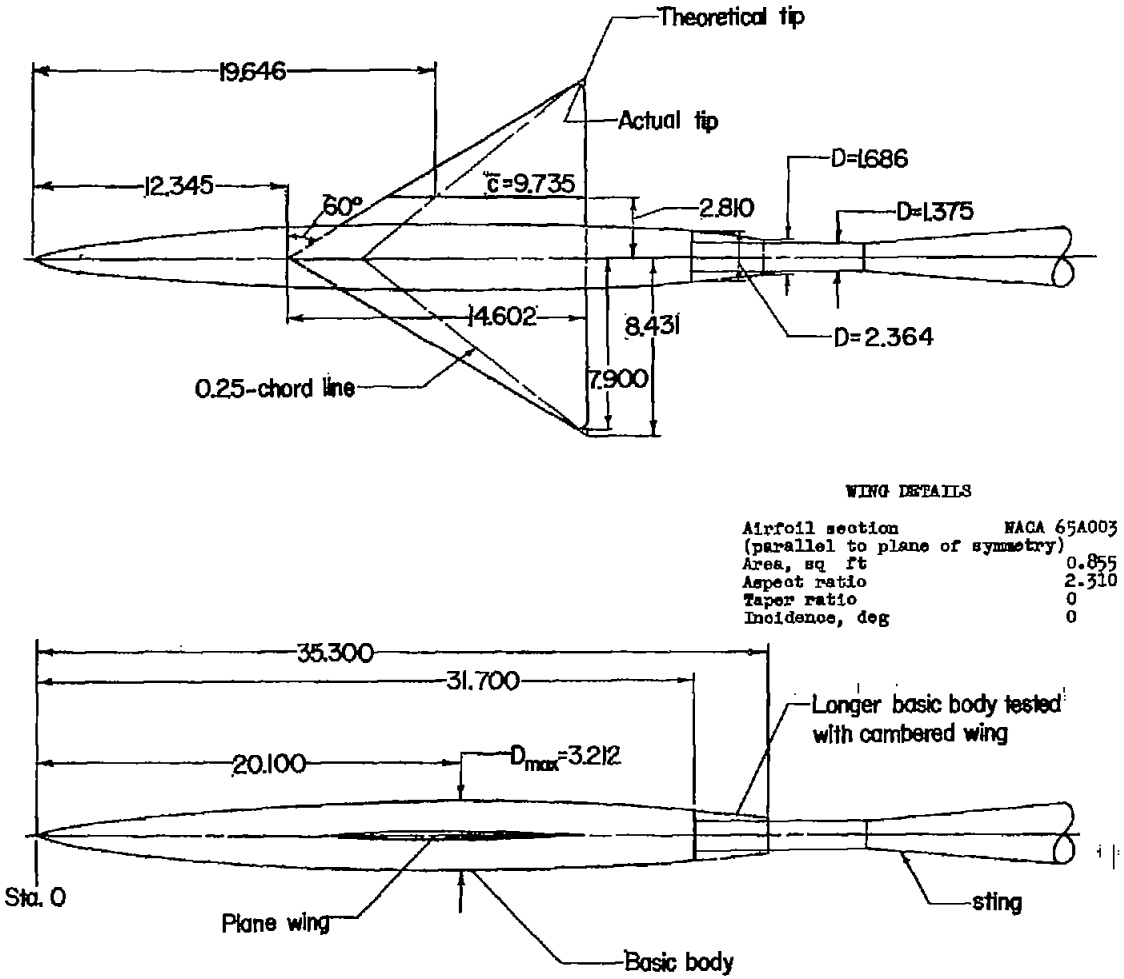


(a) Wing-body combinations.

Figure 1.- Model details. All dimensions are in inches unless otherwise noted.

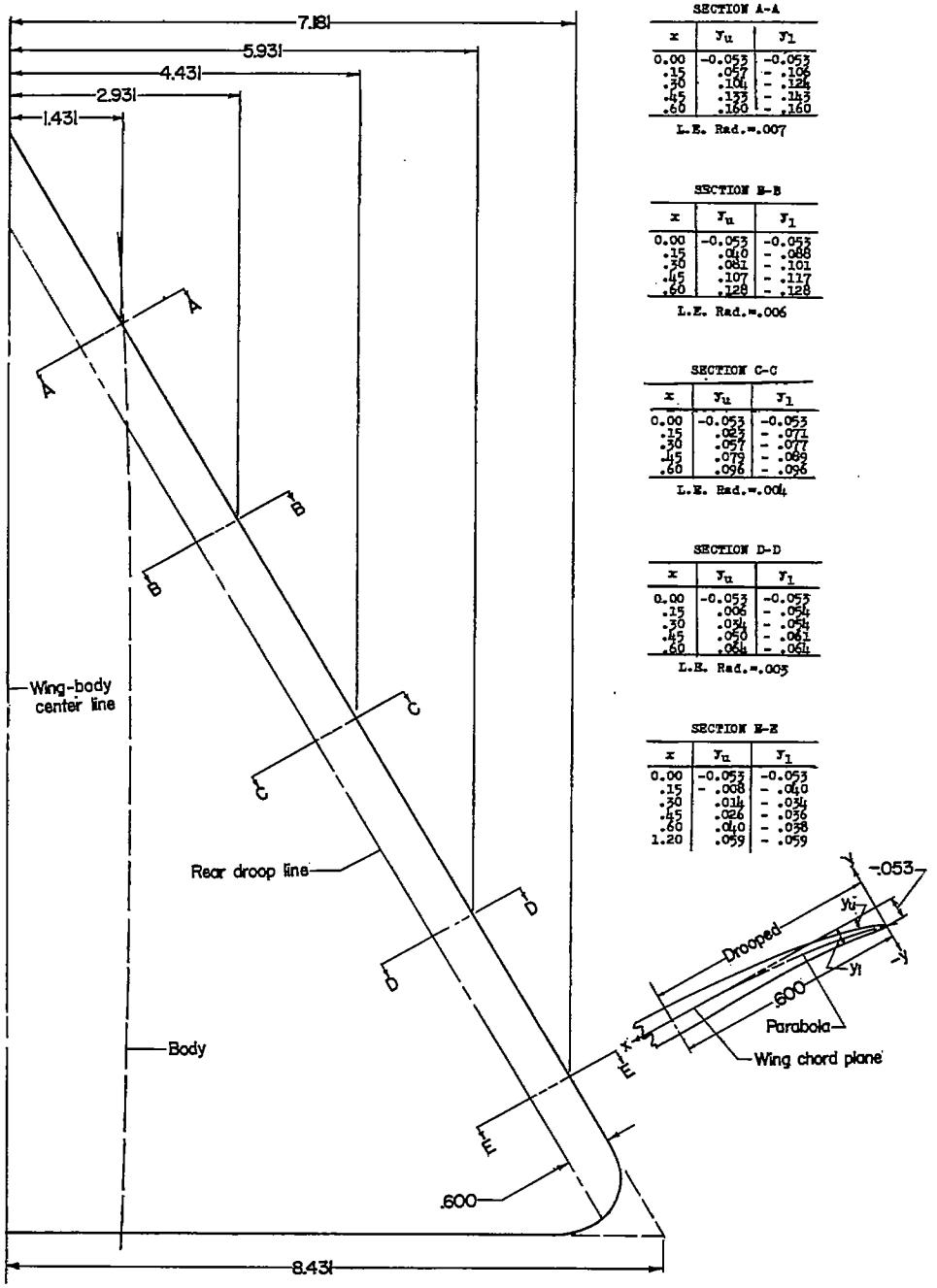


SECTION A-A

| x | $y_u$ | $y_l$ |
|---|---|---|
| 0.00 | -0.053 | -0.053 |
| .15 | .057 | - .106 |
| .30 | .101 | - .124 |
| .45 | .133 | - .143 |
| .60 | .160 | - .160 |

L.E. Rad.=.007

SECTION B-B

| x | $y_u$ | $y_l$ |
|---|---|---|
| 0.00 | -0.053 | -0.053 |
| .15 | .046 | - .088 |
| .30 | .081 | - .101 |
| .45 | .107 | - .117 |
| .60 | .128 | - .128 |

L.E. Rad.=.006

SECTION C-C

| x | $y_u$ | $y_l$ |
|---|---|---|
| 0.00 | -0.053 | -0.053 |
| .15 | .035 | - .071 |
| .30 | .057 | - .077 |
| .45 | .079 | - .089 |
| .60 | .096 | - .096 |

L.E. Rad.=.004

SECTION D-D

| x | $y_u$ | $y_l$ |
|---|---|---|
| 0.00 | -0.053 | -0.053 |
| .15 | .006 | - .054 |
| .30 | .034 | - .054 |
| .45 | .050 | - .061 |
| .60 | .064 | - .064 |

L.E. Rad.=.005

SECTION E-E

| x | $y_u$ | $y_l$ |
|---|---|---|
| 0.00 | -0.053 | -0.053 |
| .15 | - .008 | - .040 |
| .30 | .014 | - .034 |
| .45 | .026 | - .036 |
| .60 | .040 | - .038 |
| 1.20 | .059 | - .059 |

(b) Drooped leading edges. Plan form and airfoil section perpendicular to leading edge are not to same scale.

Figure 1.- Continued.

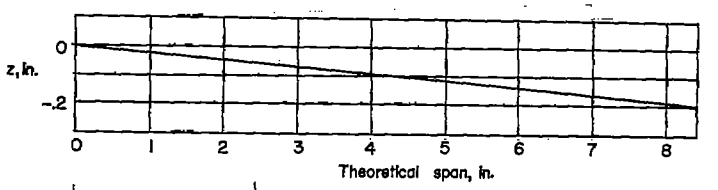


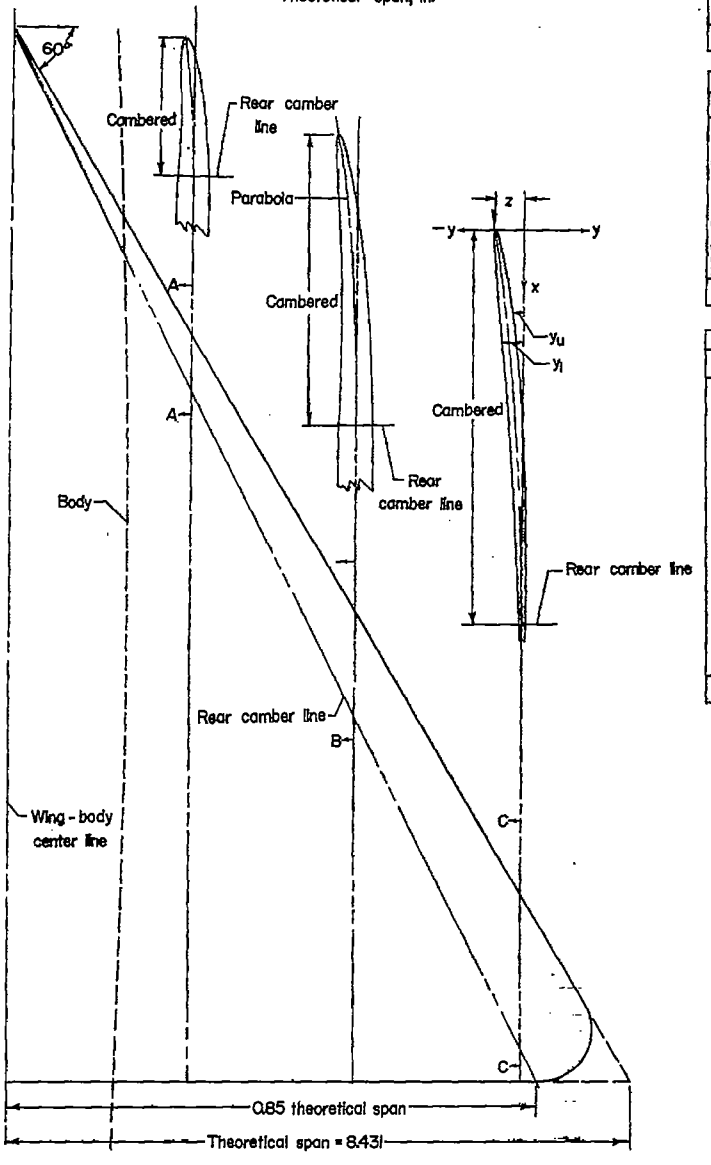


SECTION A-A

| $x_u$ | $y_u$ | $x_l$ | $y_l$ |
|---|---|---|---|
| 0 | -0.056 | 0 | -0.056 |
| 0.011 | -0.083 | 0.015 | -0.066 |
| 0.024 | -0.095 | 0.026 | -0.069 |
| 0.036 | -0.029 | 0.047 | -0.071 |
| 0.049 | -0.024 | 0.055 | -0.073 |
| 0.074 | -0.016 | 0.082 | -0.074 |
| 0.185 | -0.001 | 0.135 | -0.076 |
| 0.253 | 0.027 | 0.265 | -0.075 |
| 0.516 | 0.063 | 0.523 | -0.073 |
| 0.668 | 0.075 | 0.652 | -0.077 |

L. E. Rad. = 0.006

SECTION B-B

| $x_u$ | $y_u$ | $x_l$ | $y_l$ |
|---|---|---|---|
| 0 | -0.108 | 0 | -0.108 |
| 0.007 | -0.100 | 0.008 | -0.111 |
| 0.015 | -0.095 | 0.018 | -0.116 |
| 0.023 | -0.091 | 0.026 | -0.117 |
| 0.030 | -0.088 | 0.035 | -0.118 |
| 0.046 | -0.083 | 0.051 | -0.119 |
| 0.078 | -0.073 | 0.085 | -0.119 |
| 0.158 | -0.053 | 0.167 | -0.117 |
| 0.320 | -0.025 | 0.330 | -0.107 |
| 0.482 | 0.005 | 0.498 | -0.098 |
| 0.645 | 0.027 | 0.651 | -0.091 |
| 0.971 | 0.060 | 0.978 | -0.082 |
| 1.298 | 0.080 | 1.300 | -0.082 |

L. E. Rad. = 0.004

SECTION C-C

| $x_u$ | $y_u$ | $x_l$ | $y_l$ |
|---|---|---|---|
| 0 | -0.160 | 0 | -0.160 |
| 0.003 | -0.157 | 0.004 | -0.161 |
| 0.006 | -0.155 | 0.007 | -0.163 |
| 0.009 | -0.153 | 0.011 | -0.164 |
| 0.012 | -0.152 | 0.014 | -0.163 |
| 0.018 | -0.150 | 0.021 | -0.164 |
| 0.031 | -0.146 | 0.034 | -0.162 |
| 0.063 | -0.137 | 0.067 | -0.163 |
| 0.128 | -0.124 | 0.132 | -0.158 |
| 0.191 | -0.111 | 0.197 | -0.152 |
| 0.257 | -0.100 | 0.263 | -0.147 |
| 0.386 | -0.078 | 0.393 | -0.135 |
| 0.516 | -0.059 | 0.523 | -0.123 |
| 0.646 | -0.042 | 0.653 | -0.113 |
| 0.776 | -0.027 | 0.783 | -0.101 |
| 0.906 | -0.014 | 0.913 | -0.090 |
| 1.037 | -0.003 | 1.043 | -0.080 |
| 1.167 | 0.007 | 1.172 | -0.071 |
| 1.297 | 0.014 | 1.302 | -0.062 |
| 1.428 | 0.020 | 1.431 | -0.053 |
| 1.558 | 0.023 | 1.561 | -0.045 |
| 1.688 | 0.024 | 1.690 | -0.038 |
| 1.819 | 0.024 | 1.820 | -0.031 |
| 1.949 | 0.022 | 1.949 | -0.024 |
| 2.079 | 0.019 | 2.079 | -0.019 |

L. E. Rad. = 0.002

(c) Conical cambered leading edges. Plan form and streamwise airfoil sections are not to same scale.

Figure 1.- Concluded.

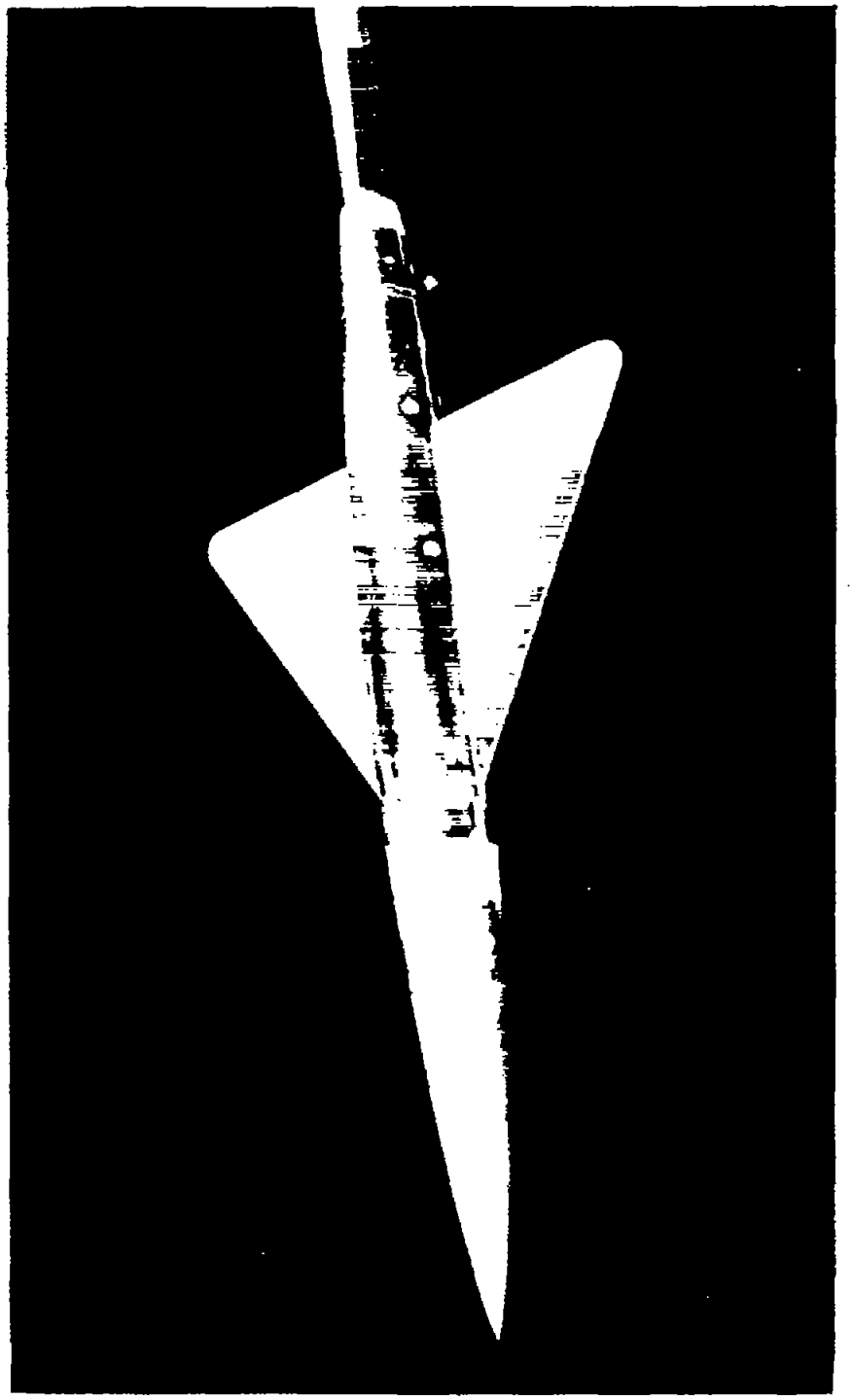

L-89623

(a) Conical cambered leading-edge wing with basic body.

Figure 2.- Photographs of model.

L-89615

(b) Conical cambered leading-edge wing with M = 1.0 indented body.

Figure 2.- Concluded.

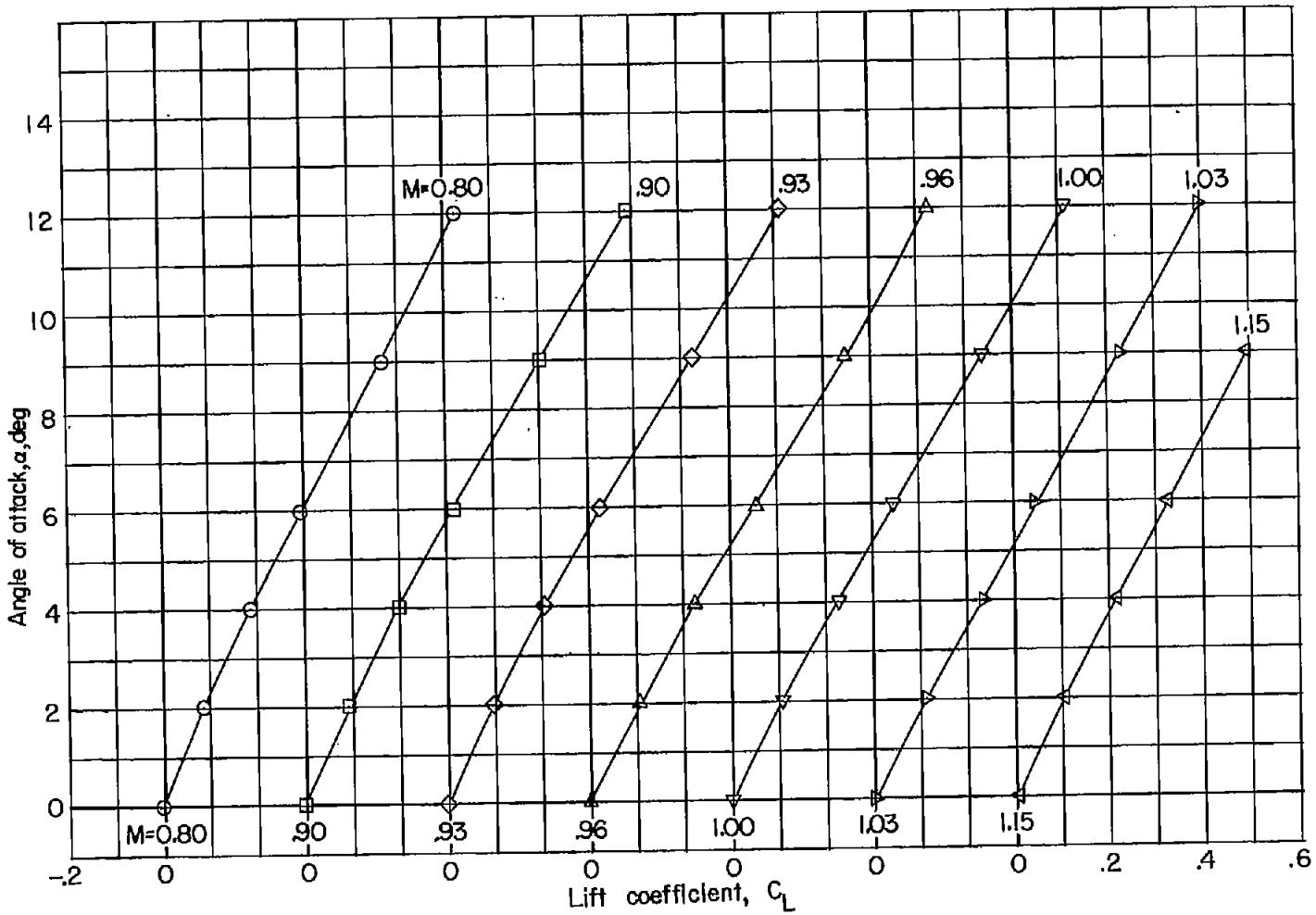


(a) Angle of attack.

Figure 3.- Aerodynamic characteristics of the plane wing-body combination. Original body.

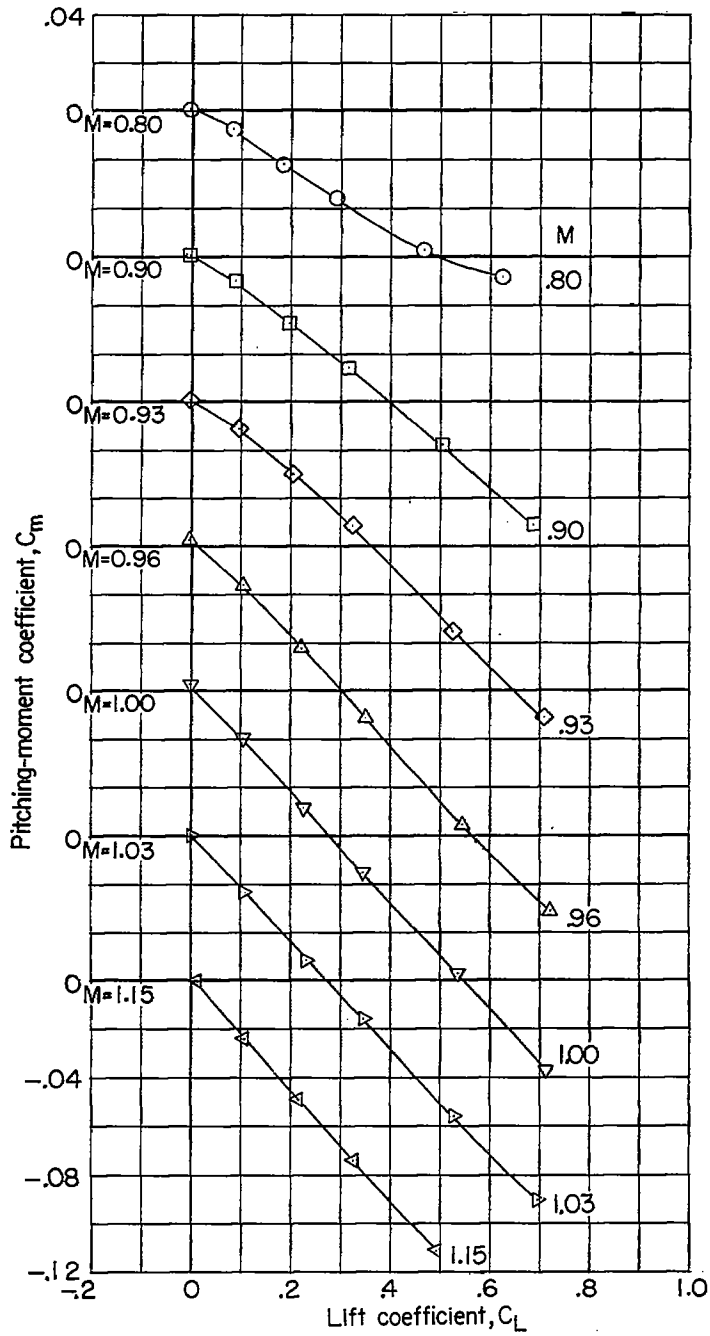


(b) Pitching-moment coefficient.

Figure 3.- Continued.

[redacted]

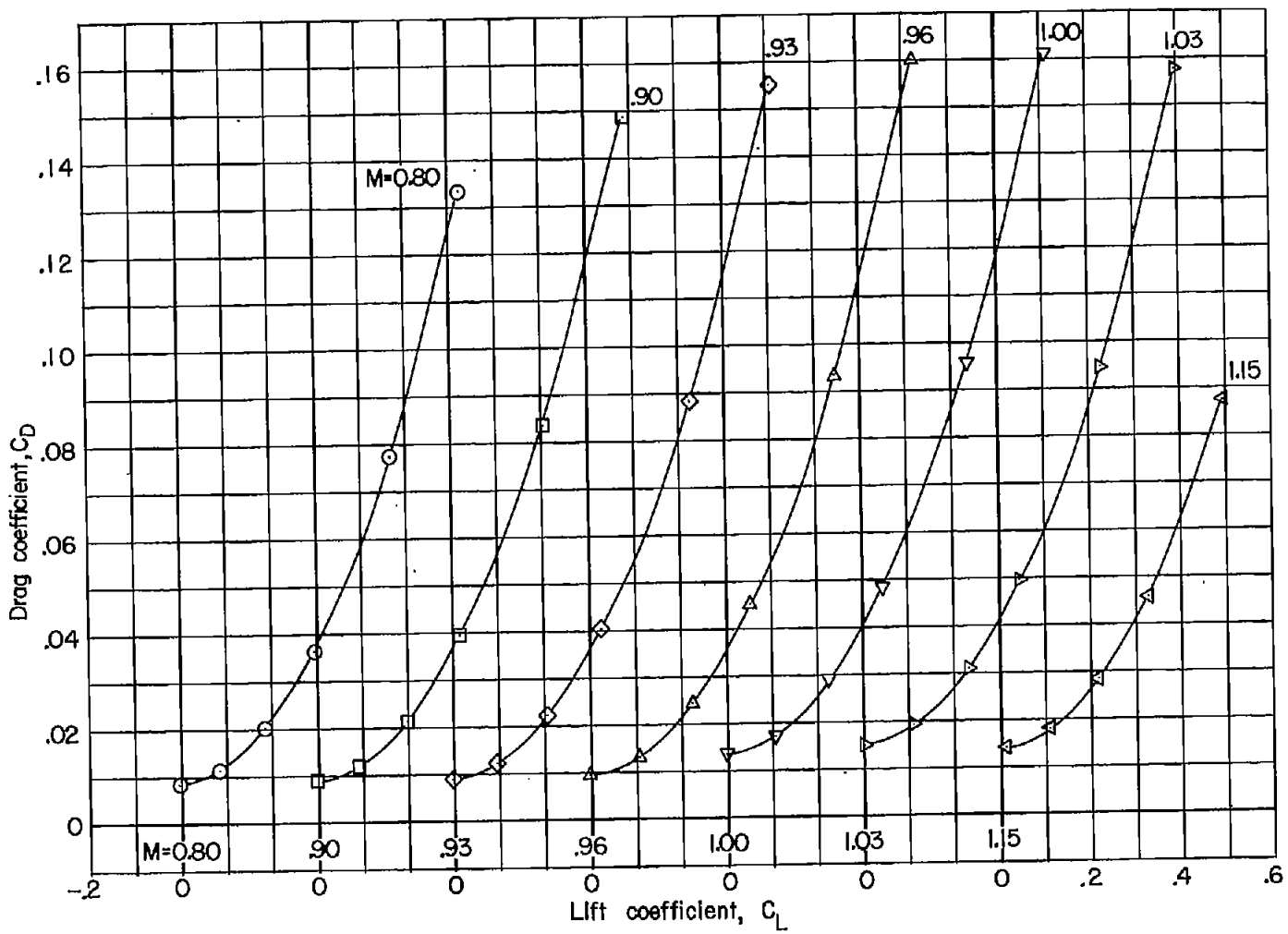


(c) Drag coefficient.

Figure 3.- Concluded.

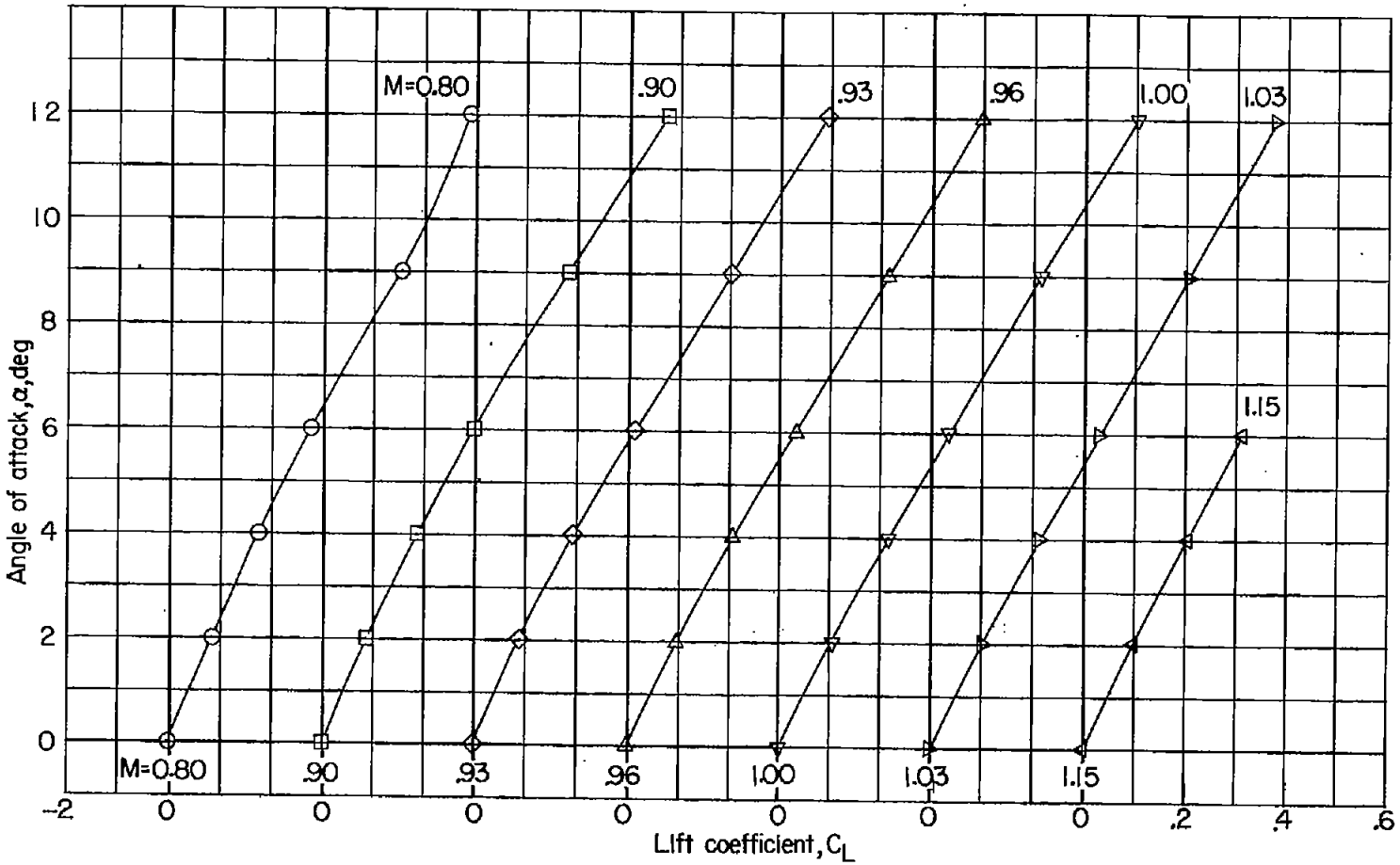


(a) Angle of attack.

Figure 4.- Aerodynamic characteristics of the wing-body combination with drooped leading edges. Original body.

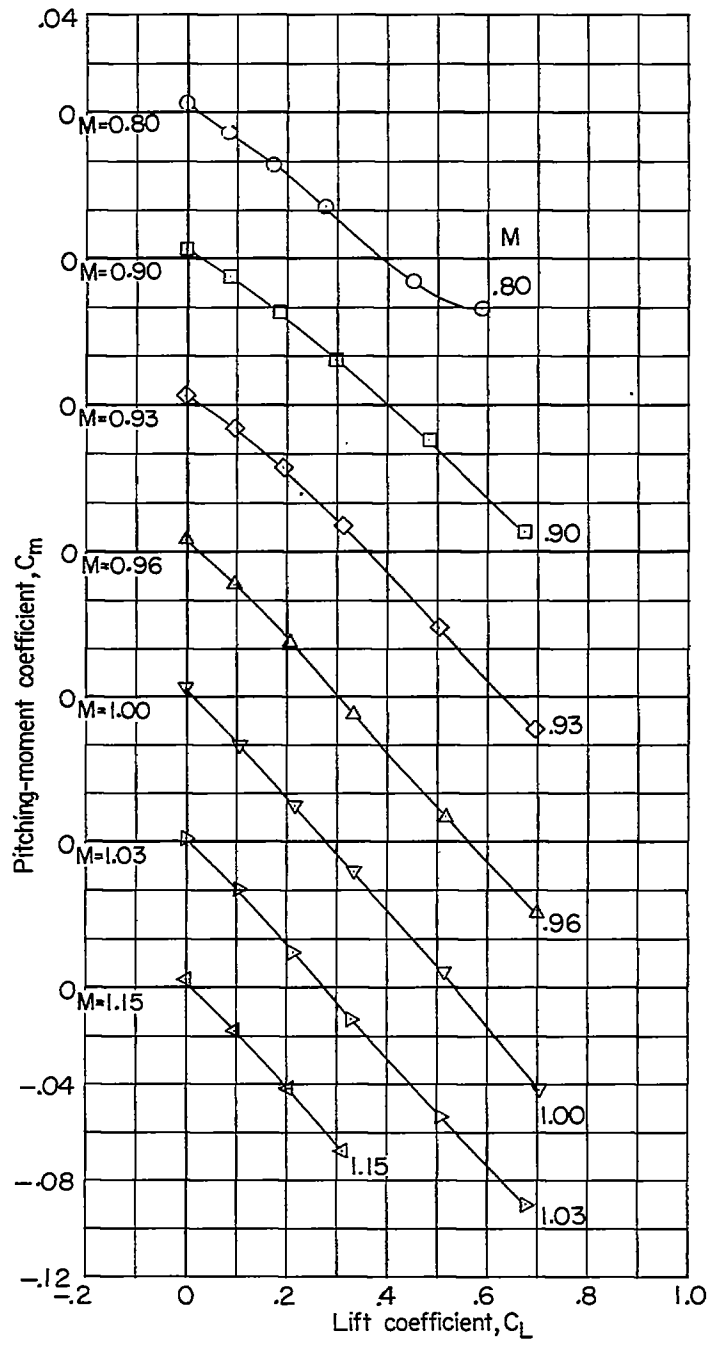


(b) Pitching-moment coefficient.

Figure 4.- Continued.

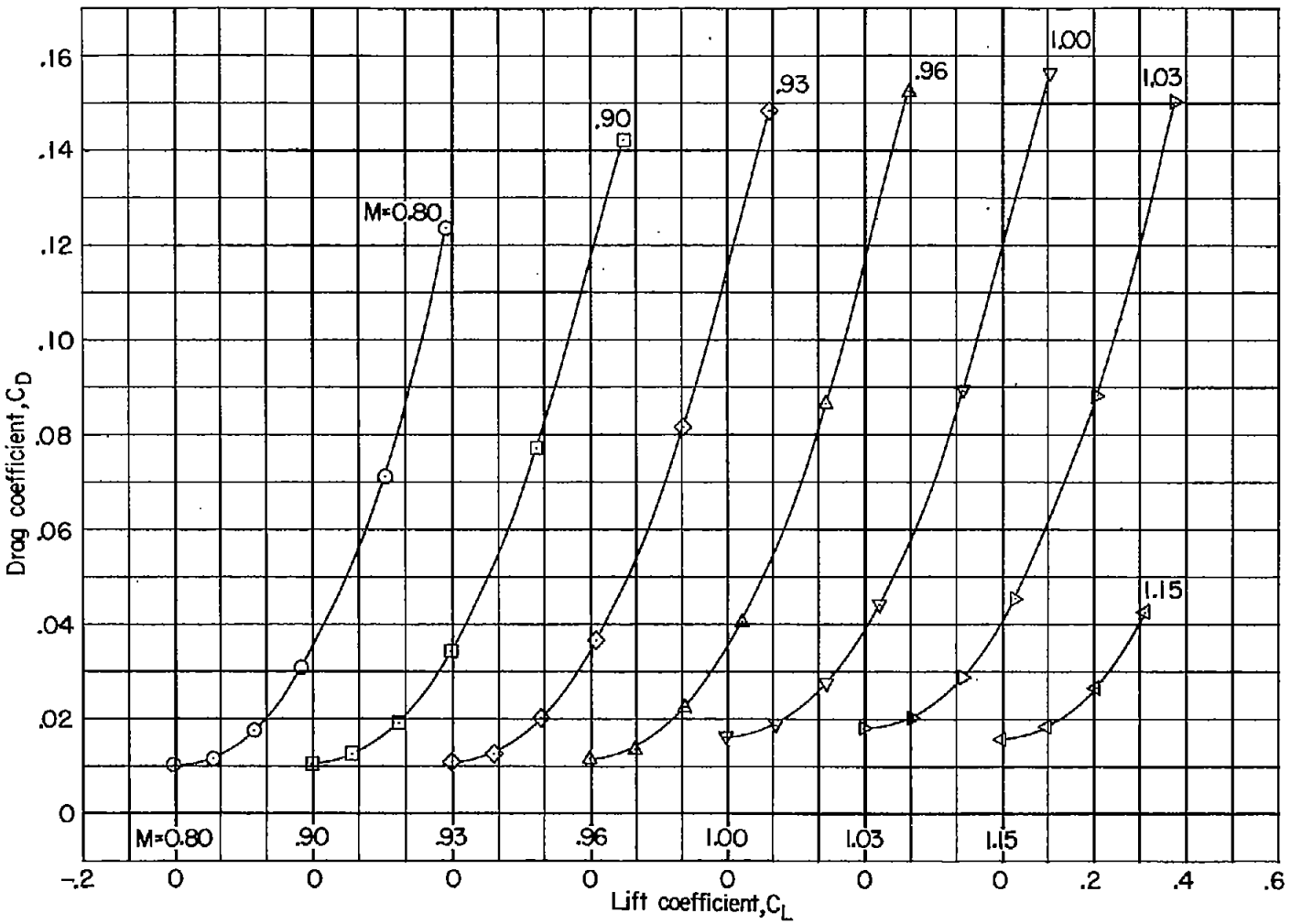


(c) Drag coefficient.

Figure 4.- Concluded.

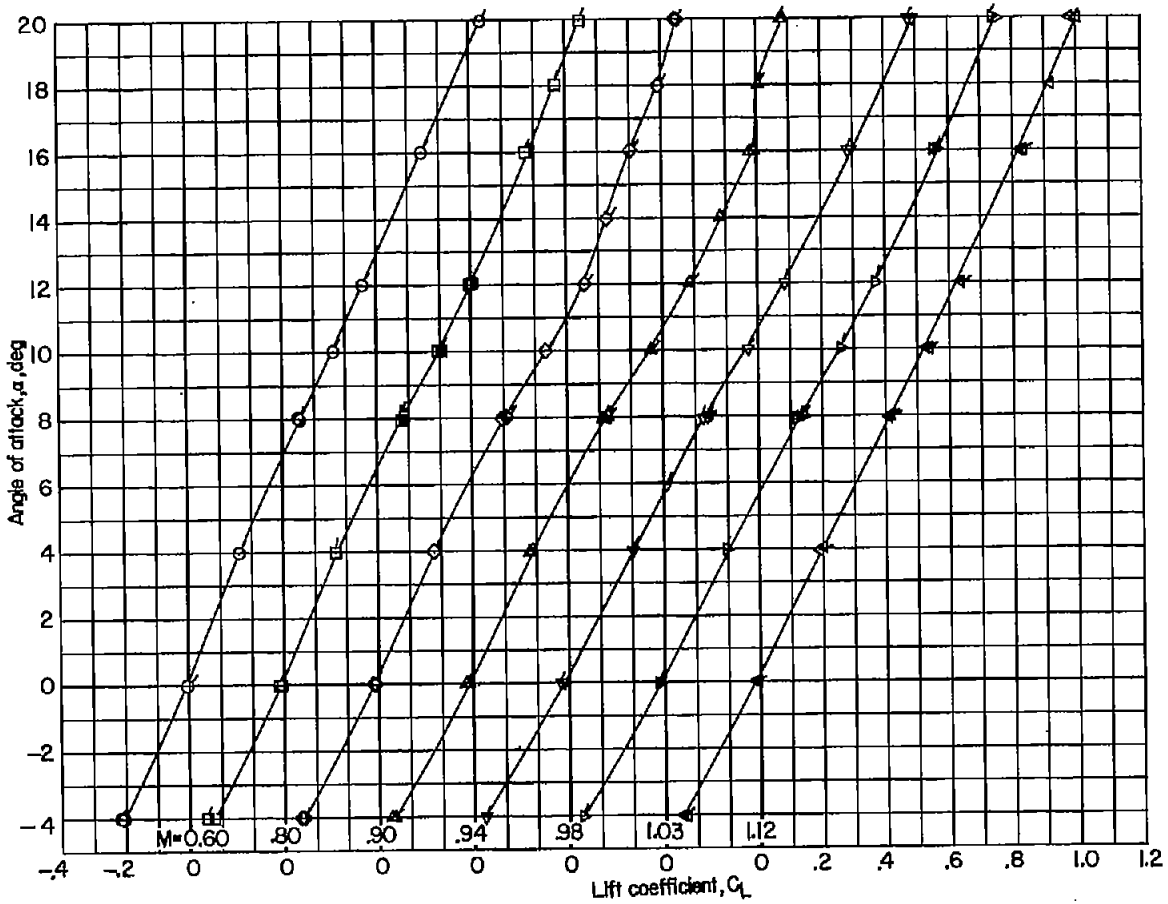


(a) Angle of attack.

Figure 5.- Aerodynamic characteristics of the wing-body combination with conical cambered leading edges. Basic body. Curves faired through plain symbols represent transition-free data; flagged symbols represent transition-fixed data.

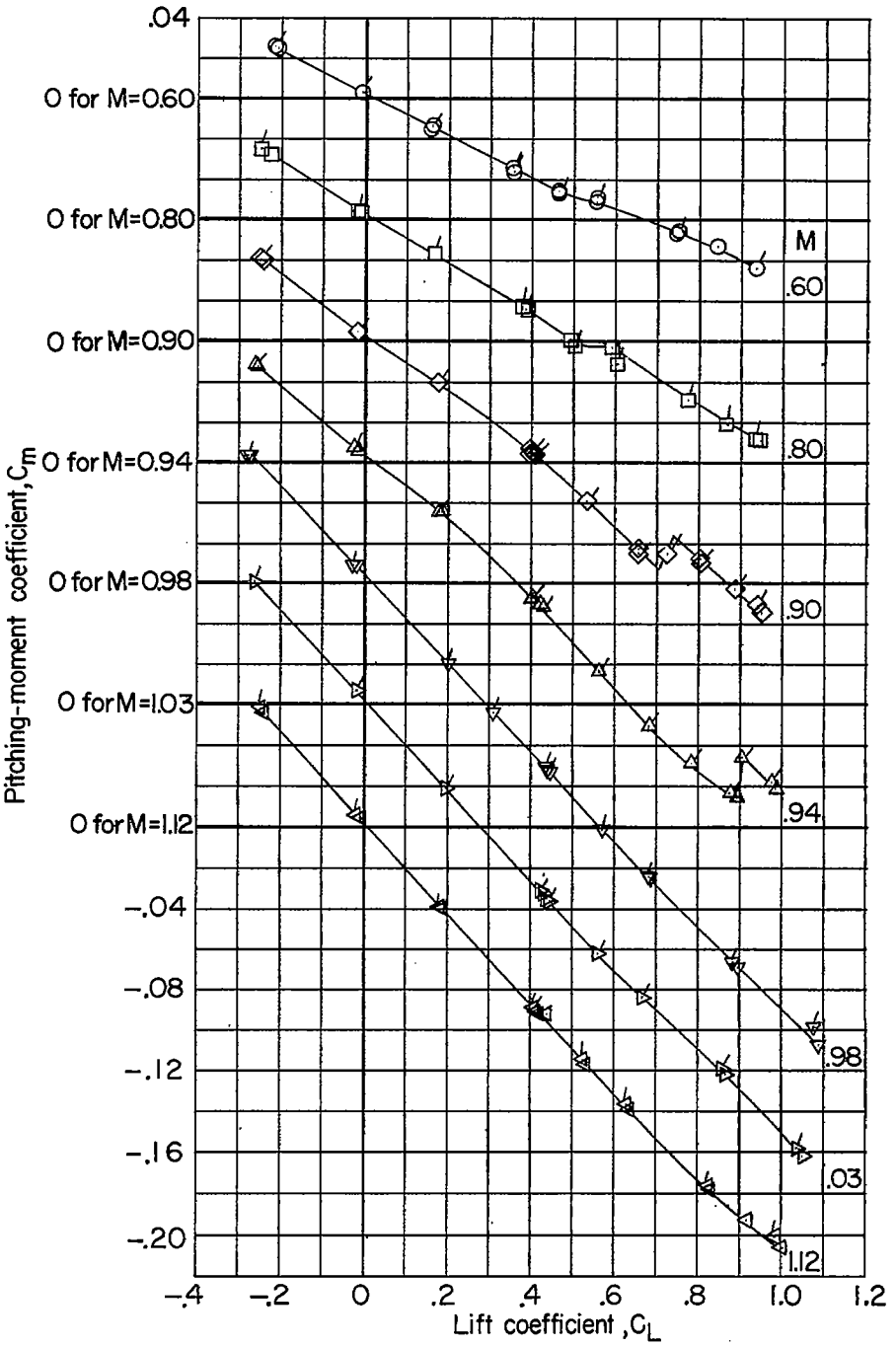


(b) Pitching-moment coefficient.

Figure 5.- Continued.

[redacted]

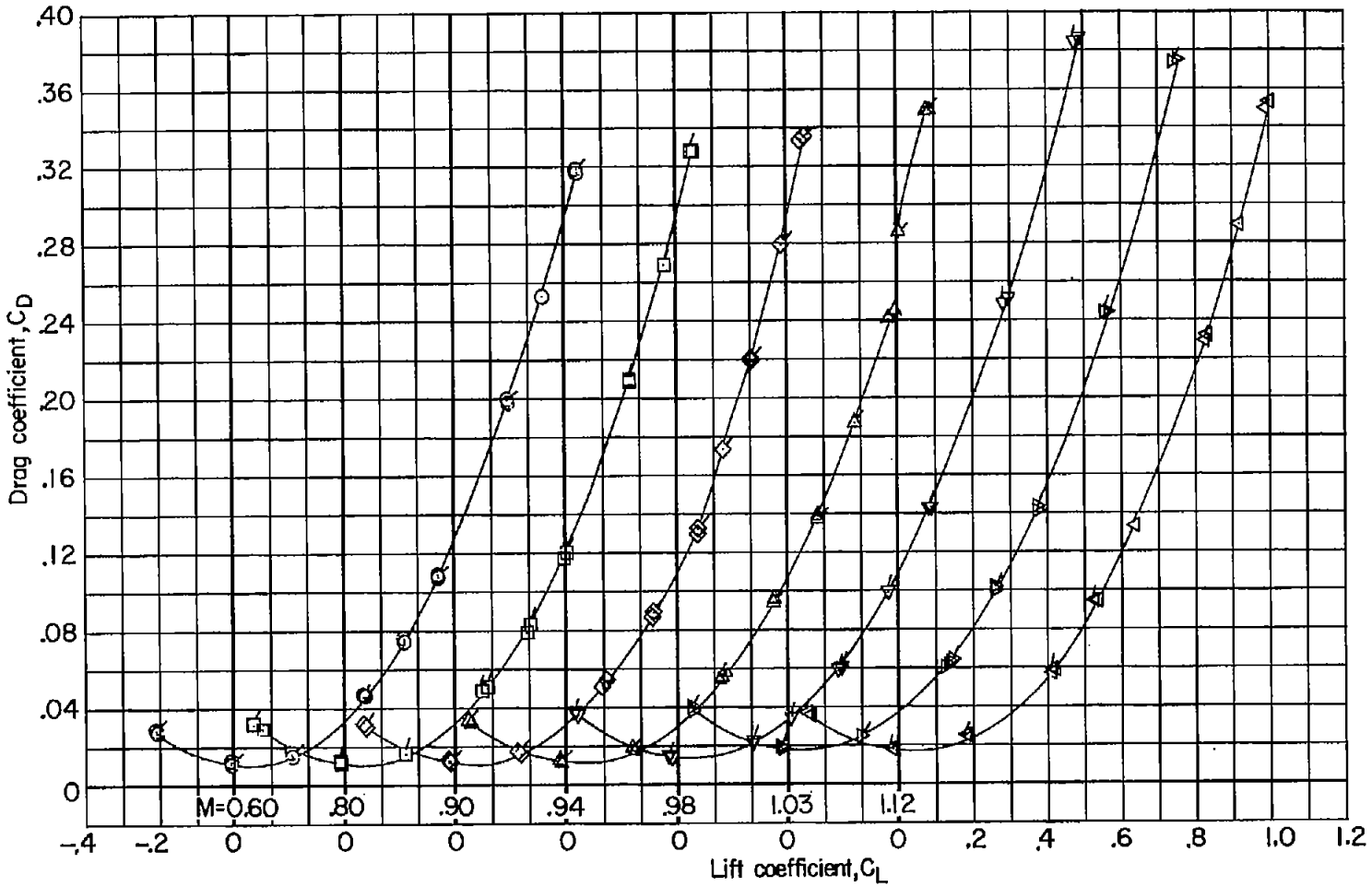


(c) Drag coefficient.

Figure 5.- Concluded.

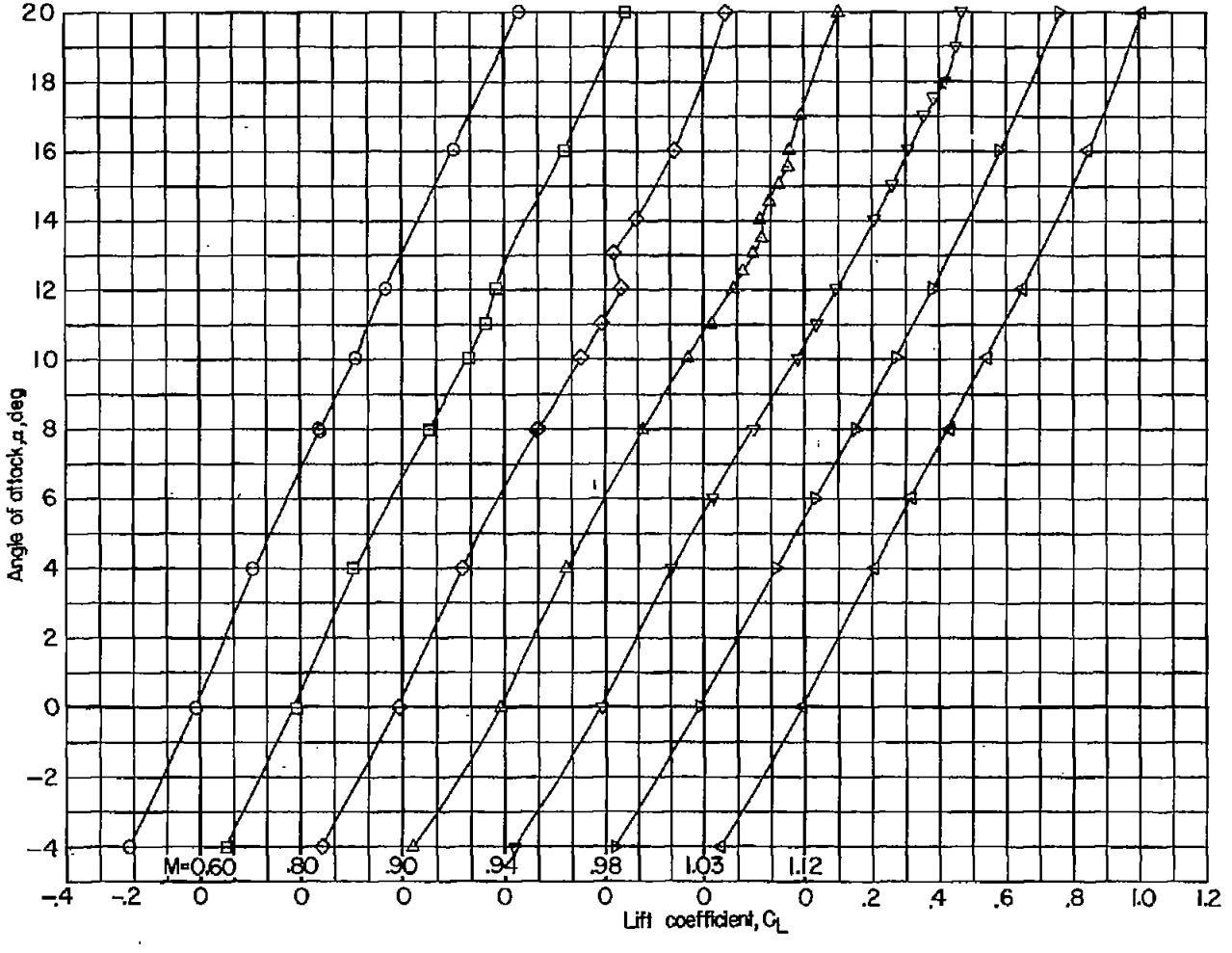


(a) Angle of attack.

Figure 6.- Aerodynamic characteristics of the wing-body combination with conical cambered leading edges. Body indented for M = 1.0.

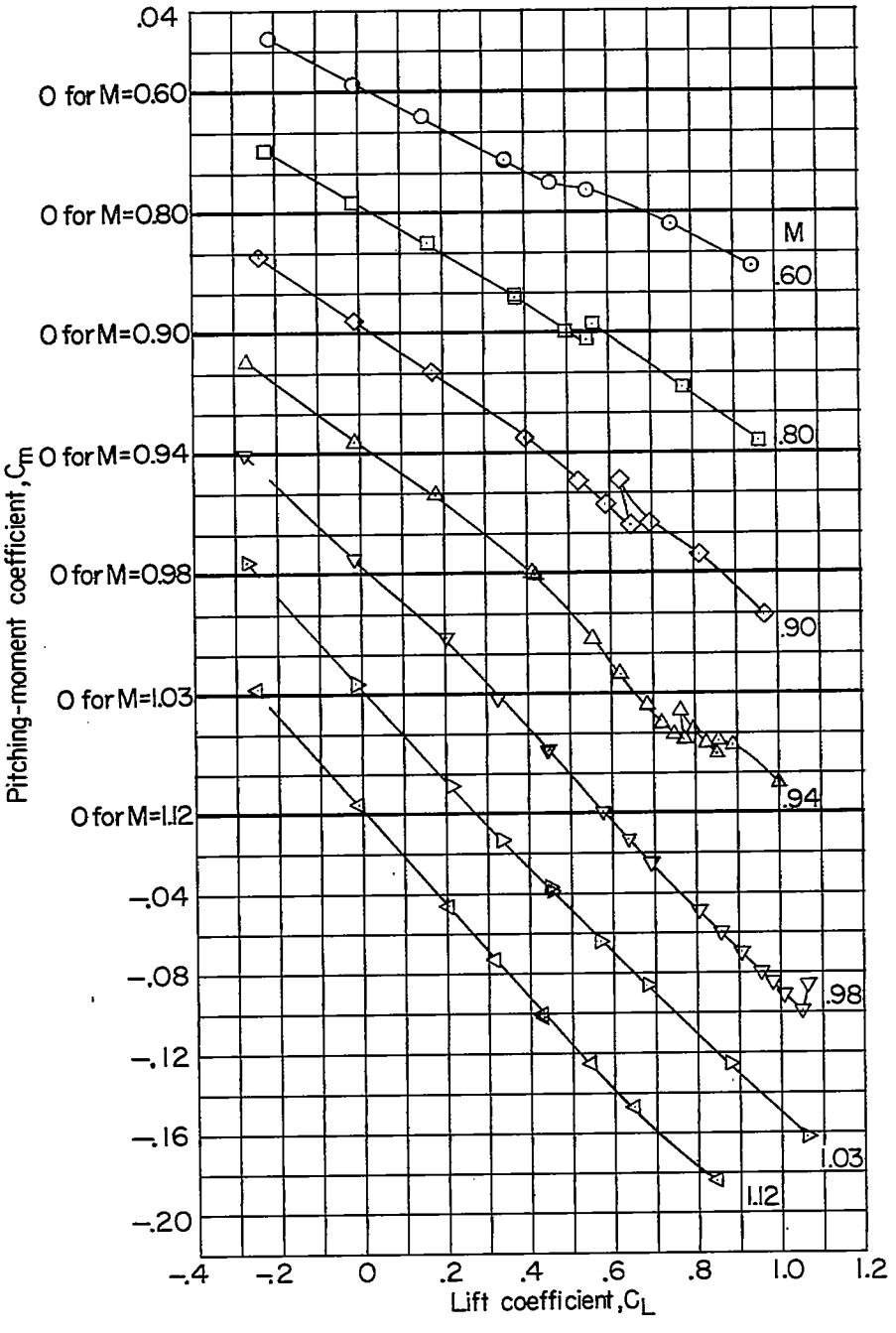


(b) Pitching-moment coefficient.

Figure 6.- Continued.

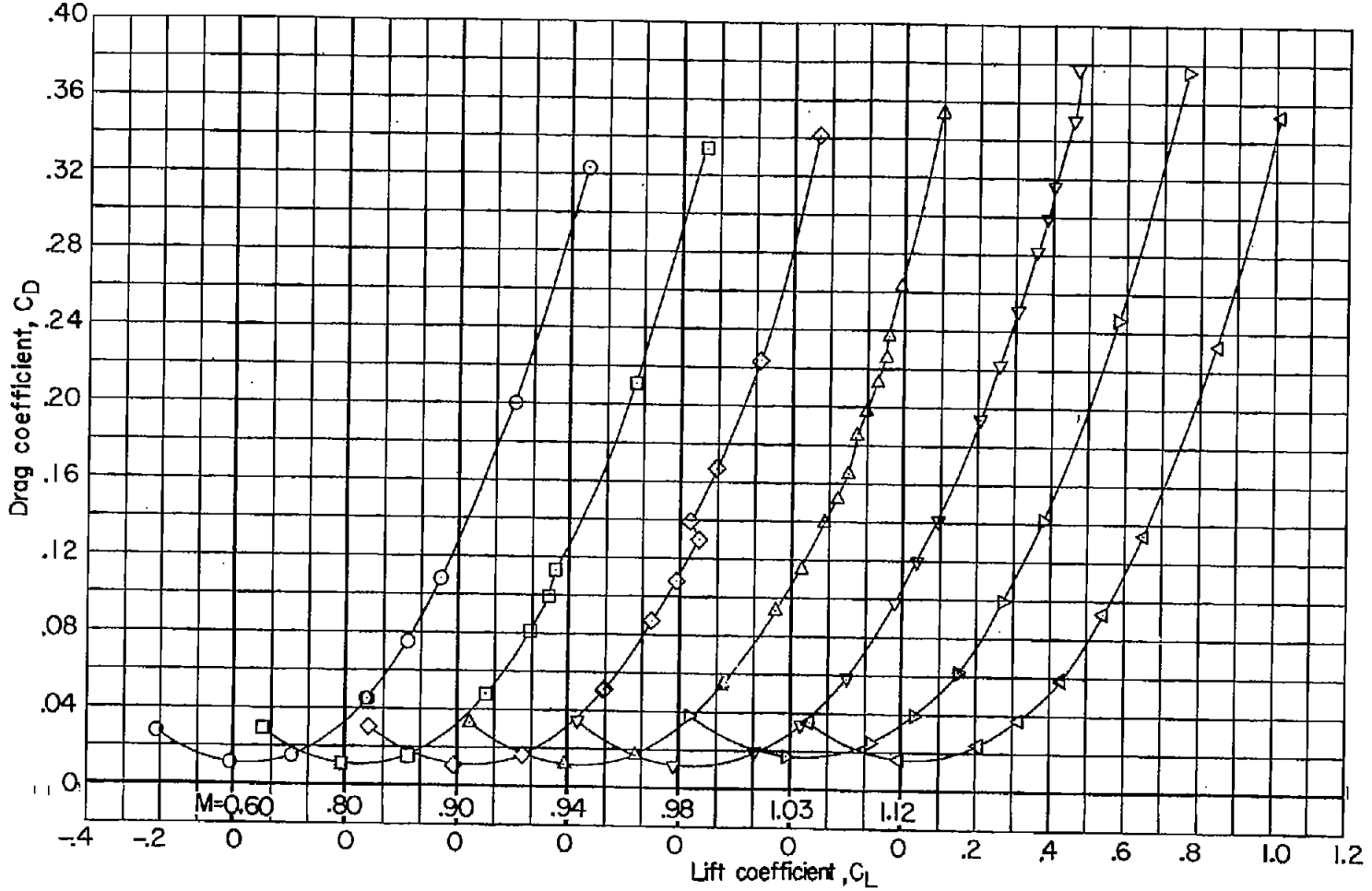


(c) Drag coefficient.

Figure 6.- Concluded.

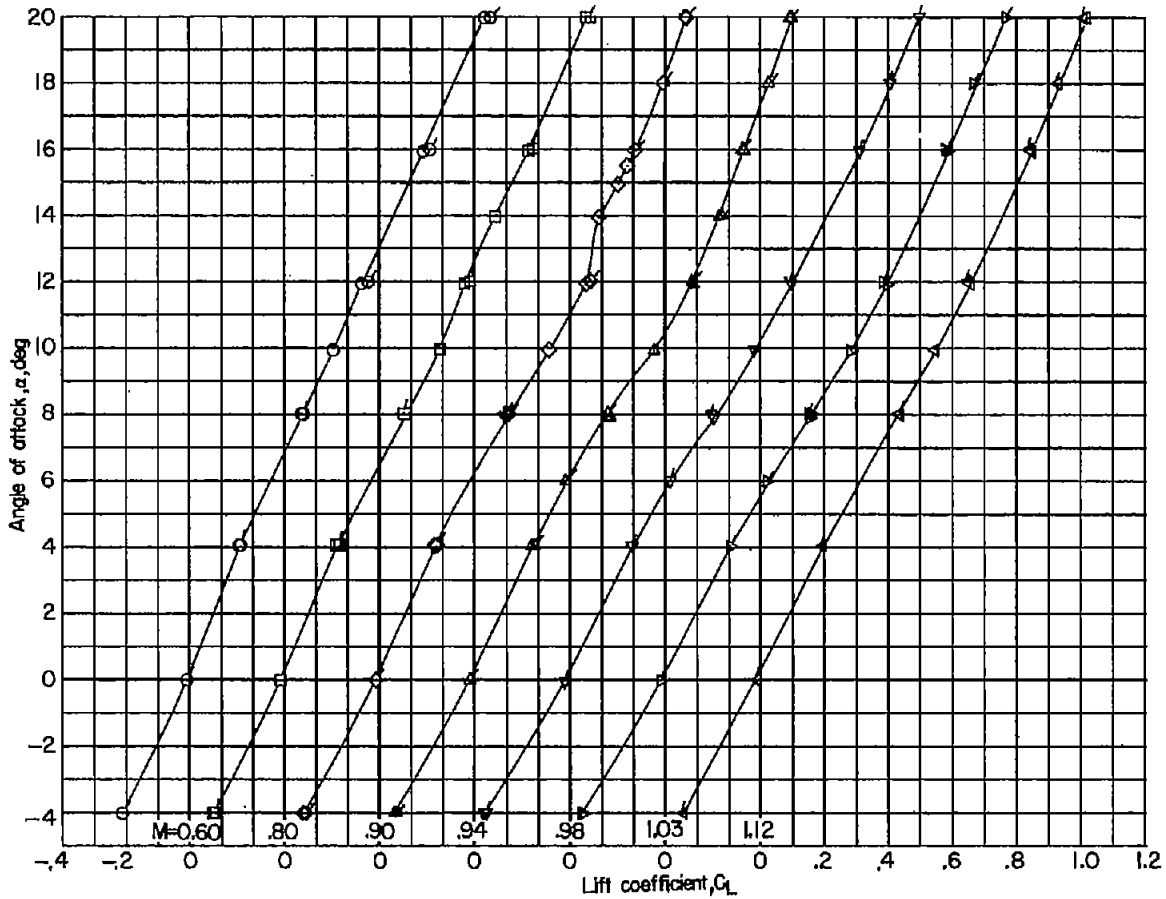


(a) Angle of attack.

Figure 7.- Aerodynamic characteristics of the wing-body combination with conical cambered leading edges. Body indented for M = 1.2. Curves faired through plain symbols represent transition-free data; flagged symbols represent transition-fixed data.

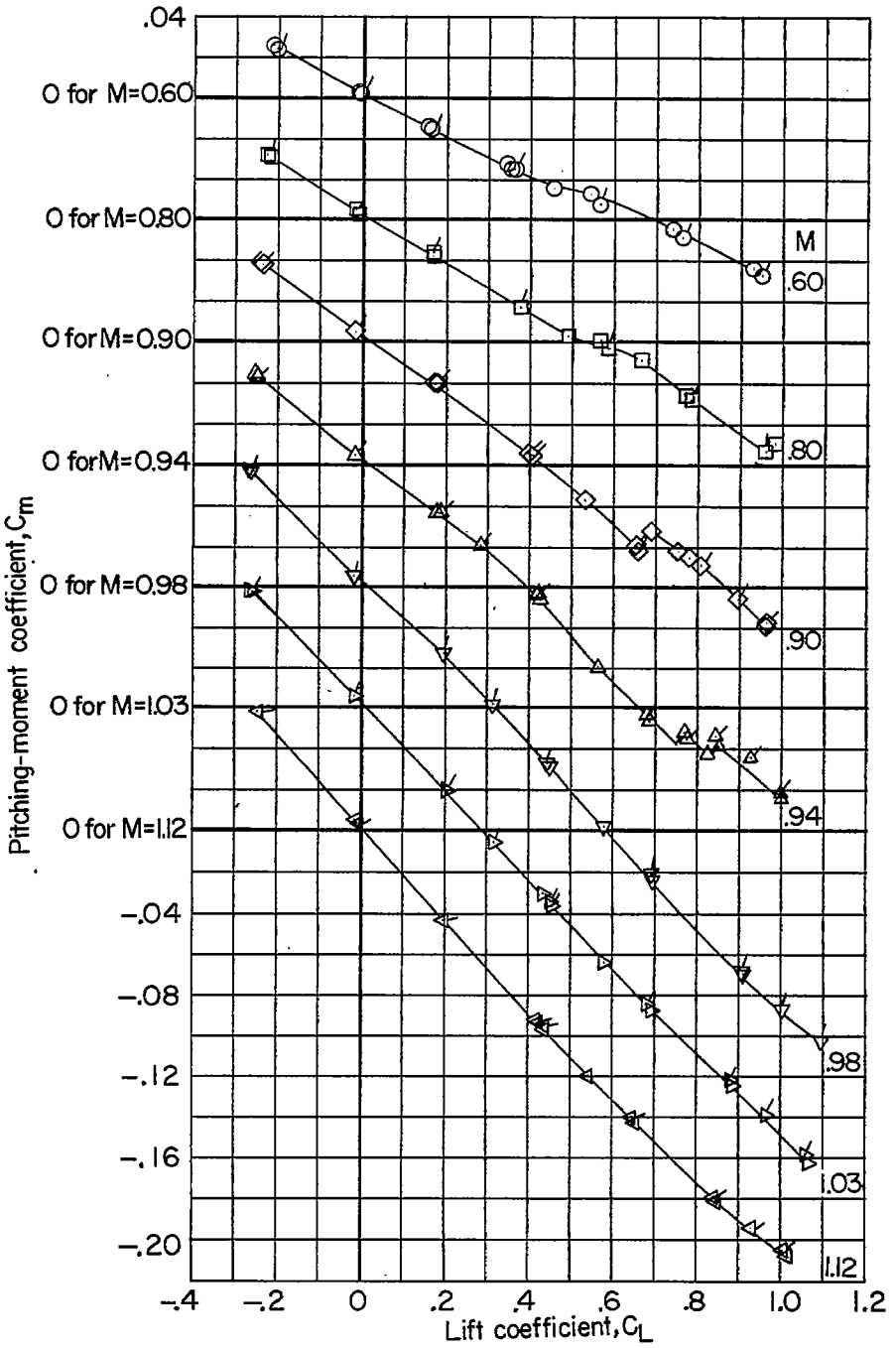


(b) Pitching-moment coefficient.

Figure 7.- Continued.

[redacted]

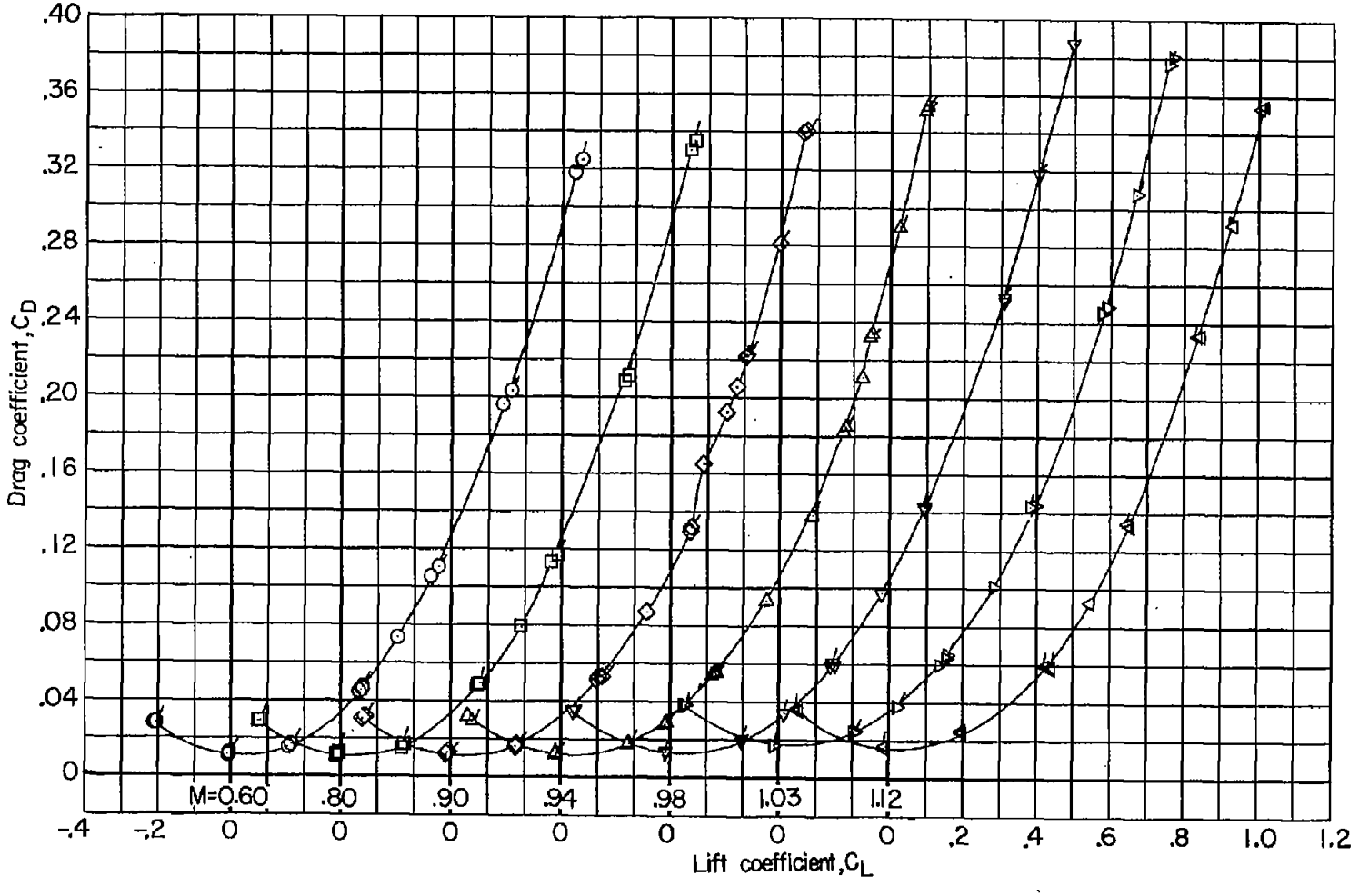


(c) Drag coefficient.

Figure 7.- Concluded.

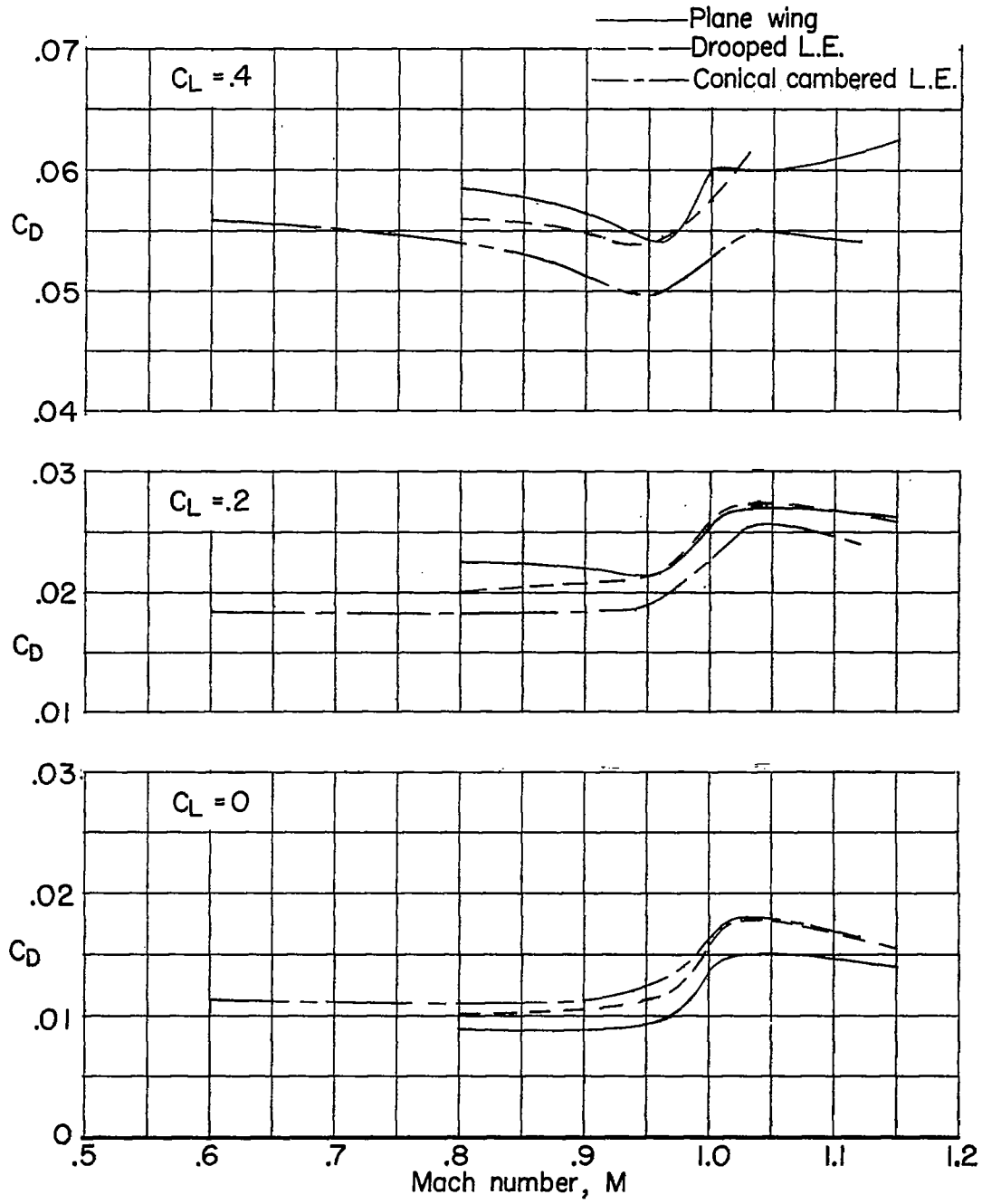


(a) Drag characteristics at several lift coefficients.

Figure 8.- Effects of leading-edge modifications on the aerodynamic parameters.

[redacted]

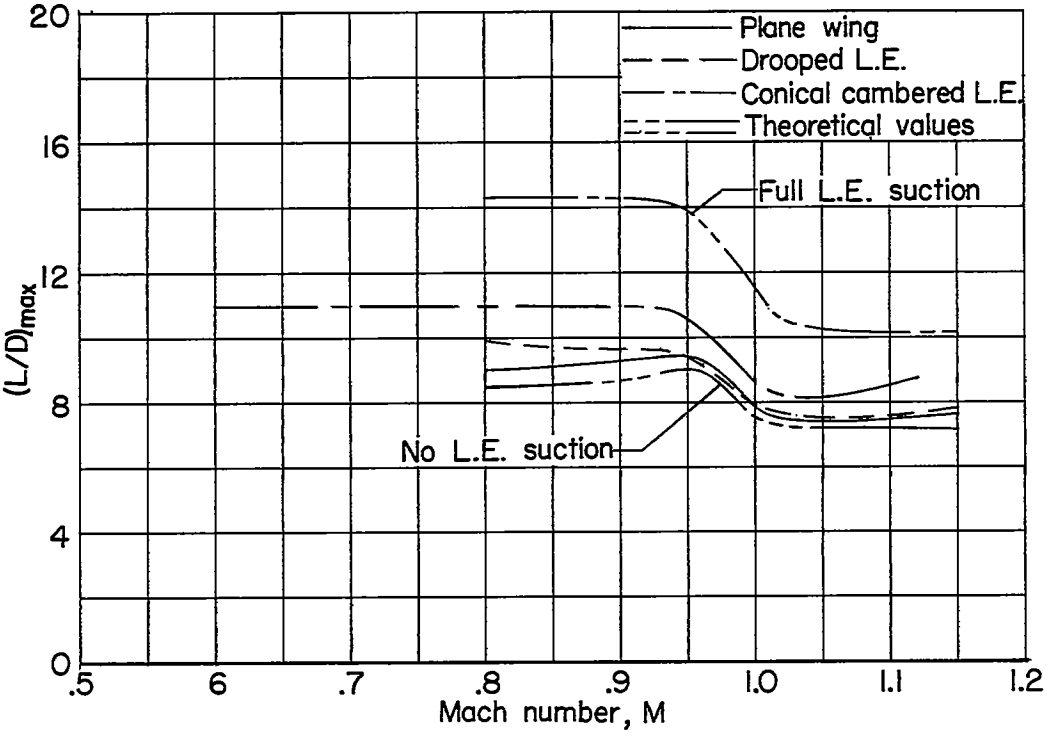


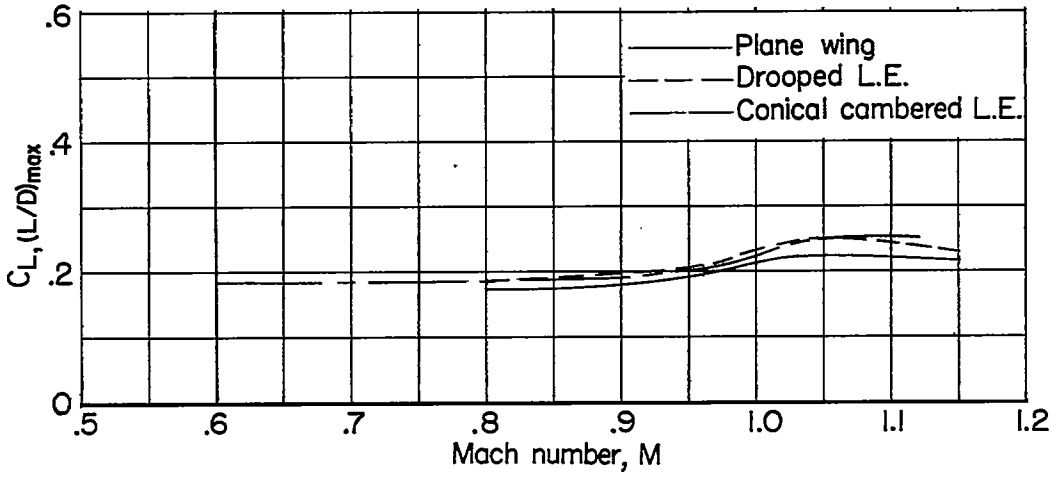


(b) Maximum lift-drag ratio characteristics.

Figure 8.- Continued.

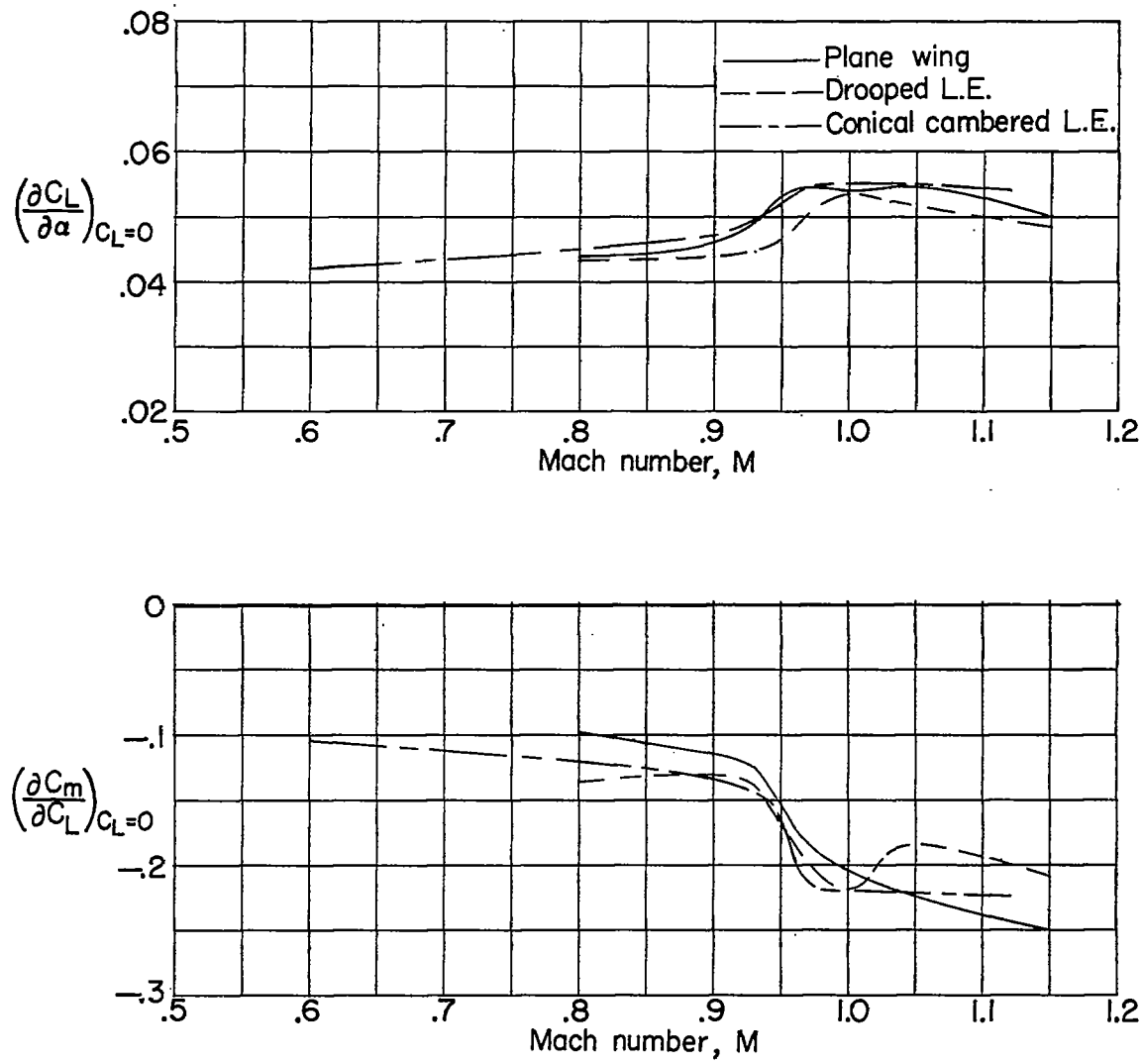


(c) Lift-curve slopes and static longitudinal stability parameter.

Figure 8.- Concluded.

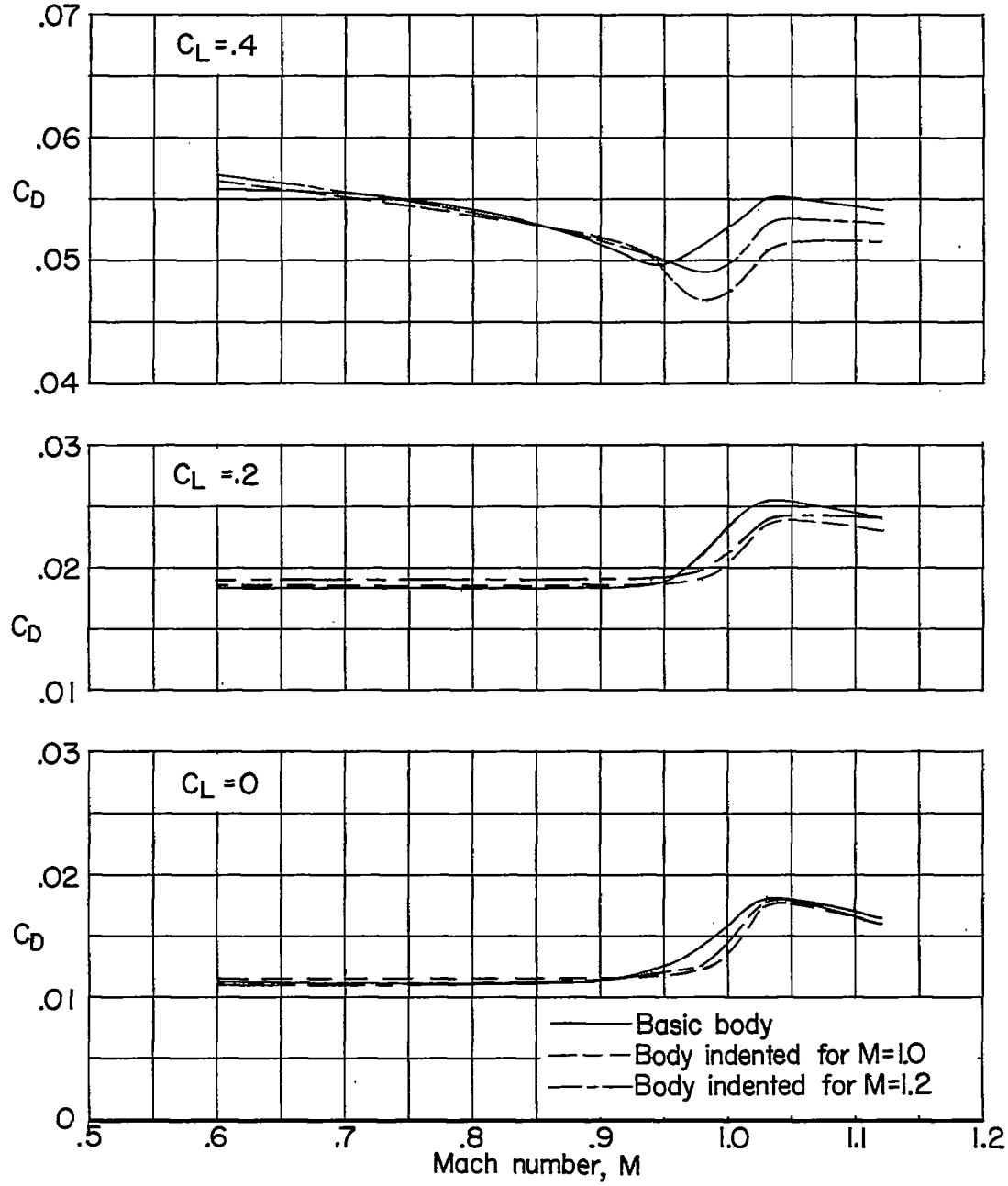


(a) Drag characteristics at several lift coefficients.

Figure 9.- Effects of body indentation on the aerodynamic parameters of the wing-body combination with conical cambered leading edges.

[redacted]

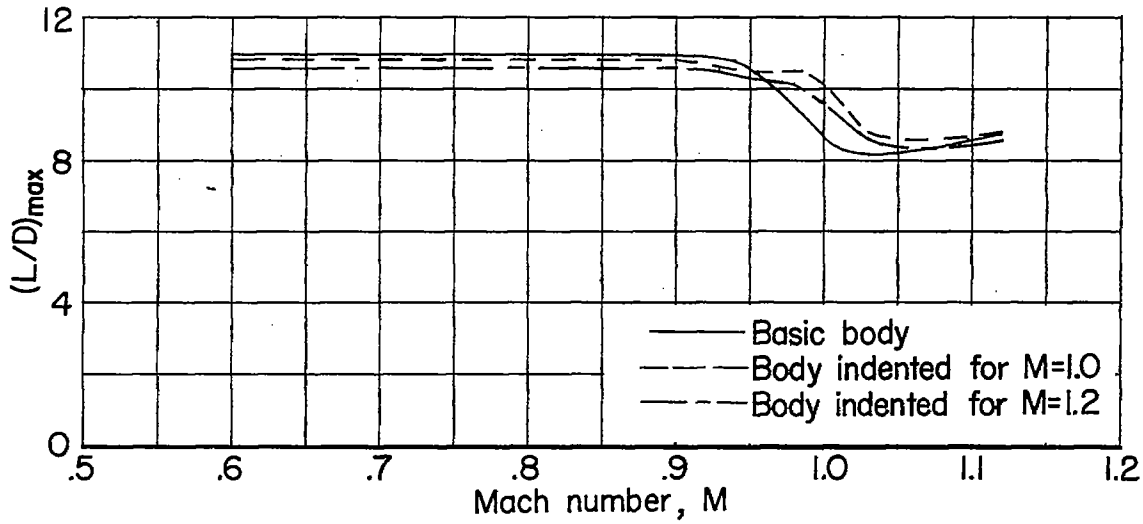


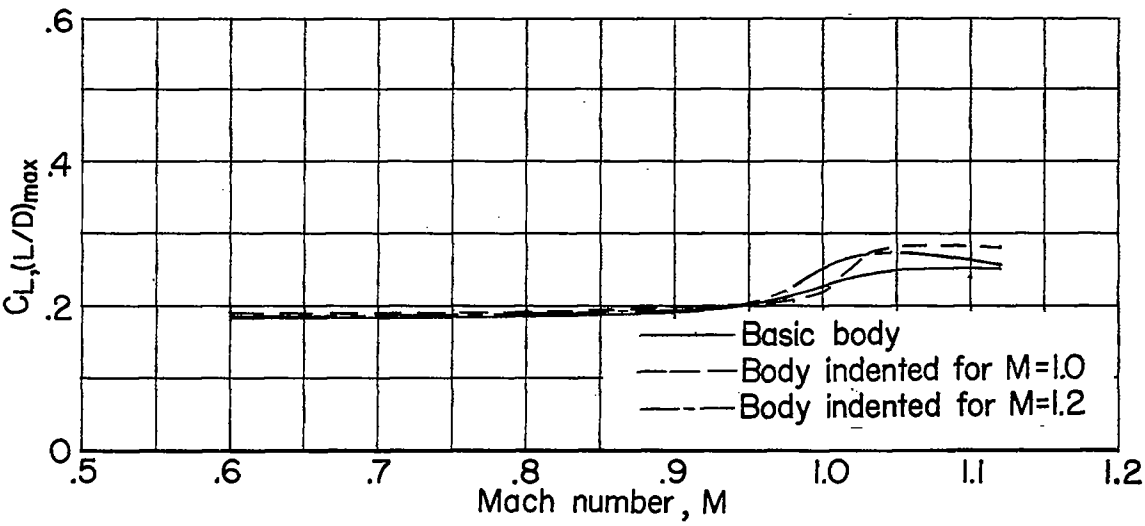


(b) Maximum lift-drag ratio characteristics.

Figure 9.- Concluded.

[redacted]

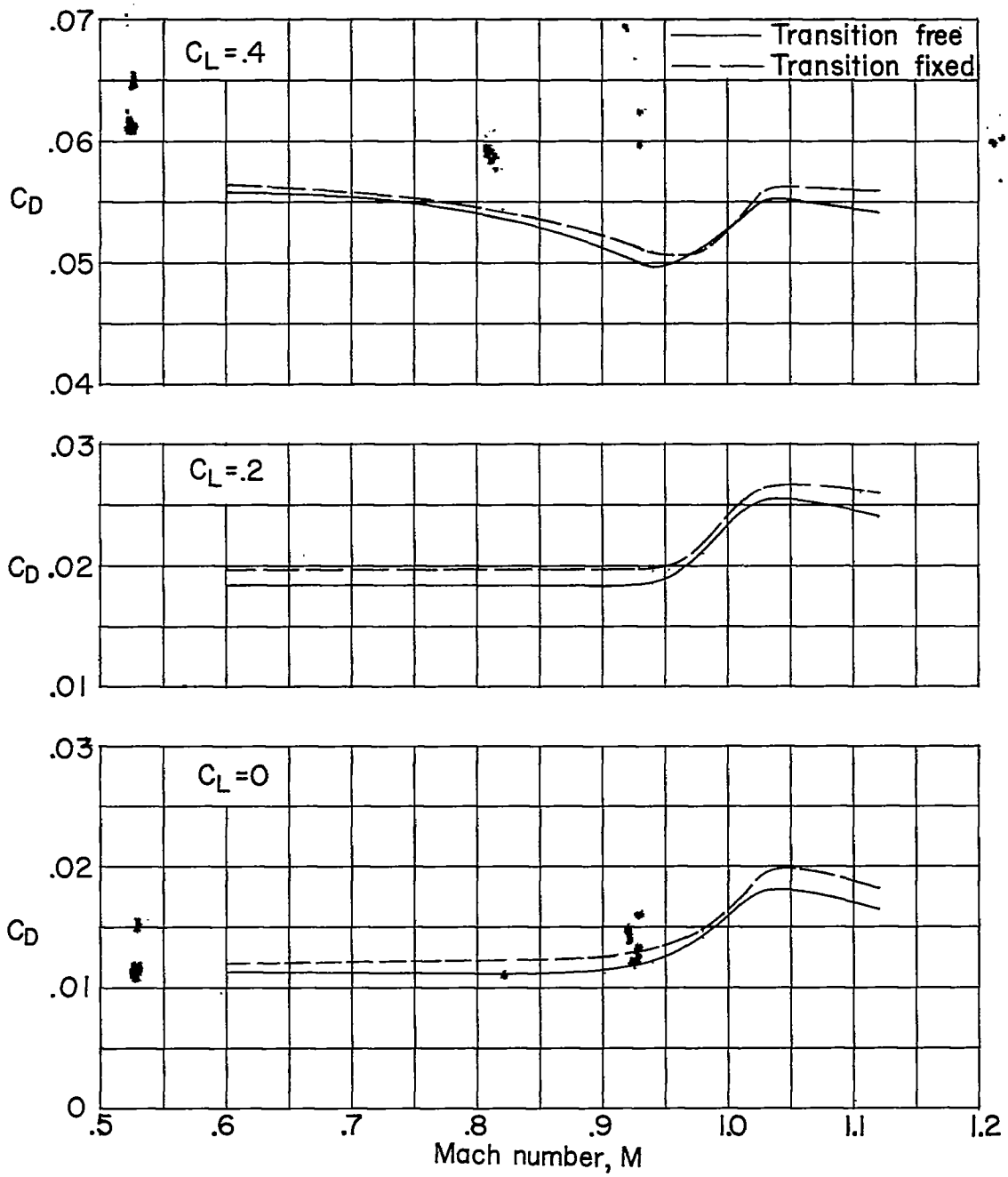


(a) Basic body.

Figure 10.- Effects of transition on the drag characteristics of the wing-body combination with conical cambered leading edges.

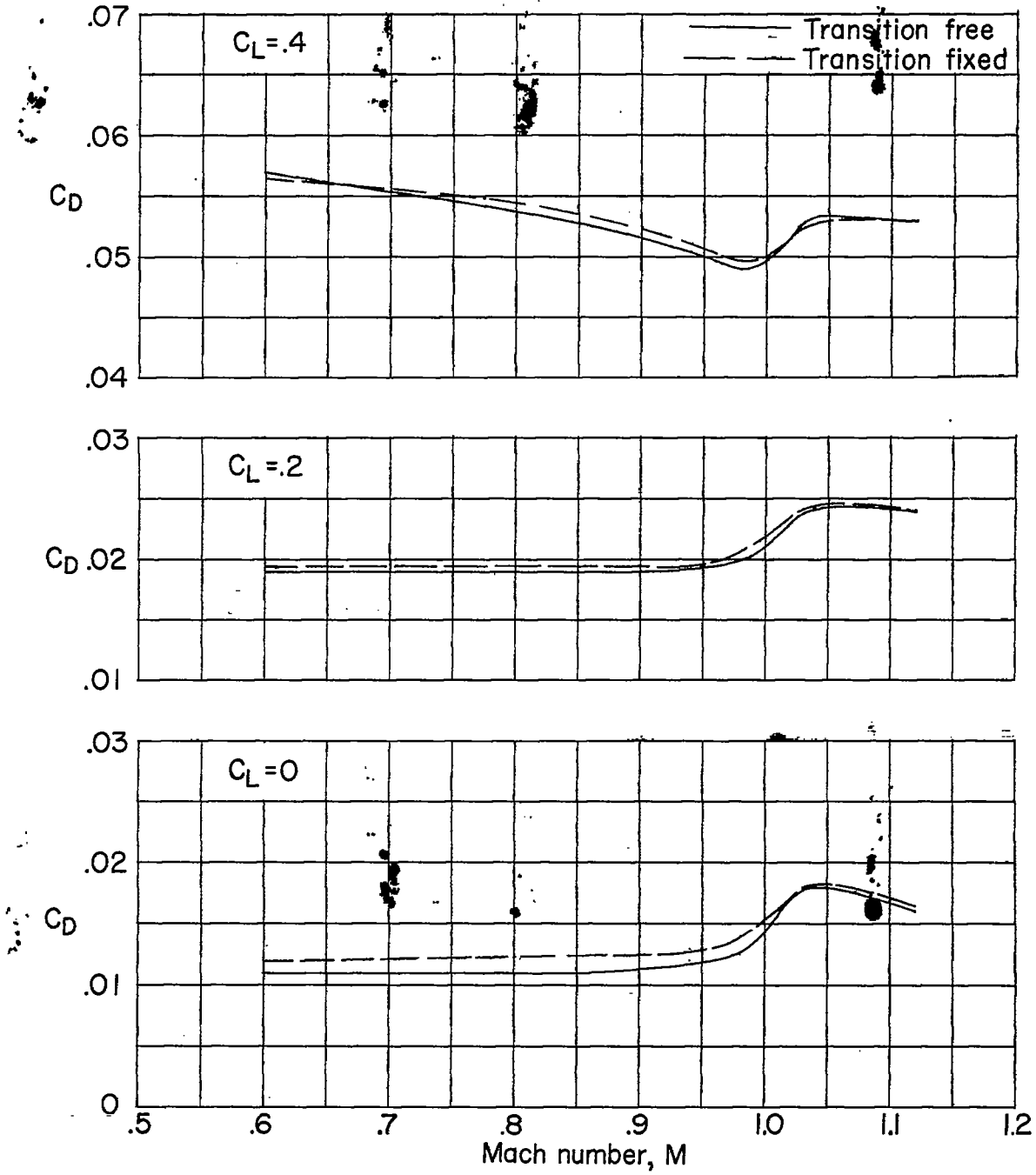


(b) Body indented for M = 1.2.

Figure 10.- Concluded.